iScience

CellPress

Article

FAM13A Represses AMPK Activity and Regulates Hepatic Glucose and Lipid Metabolism

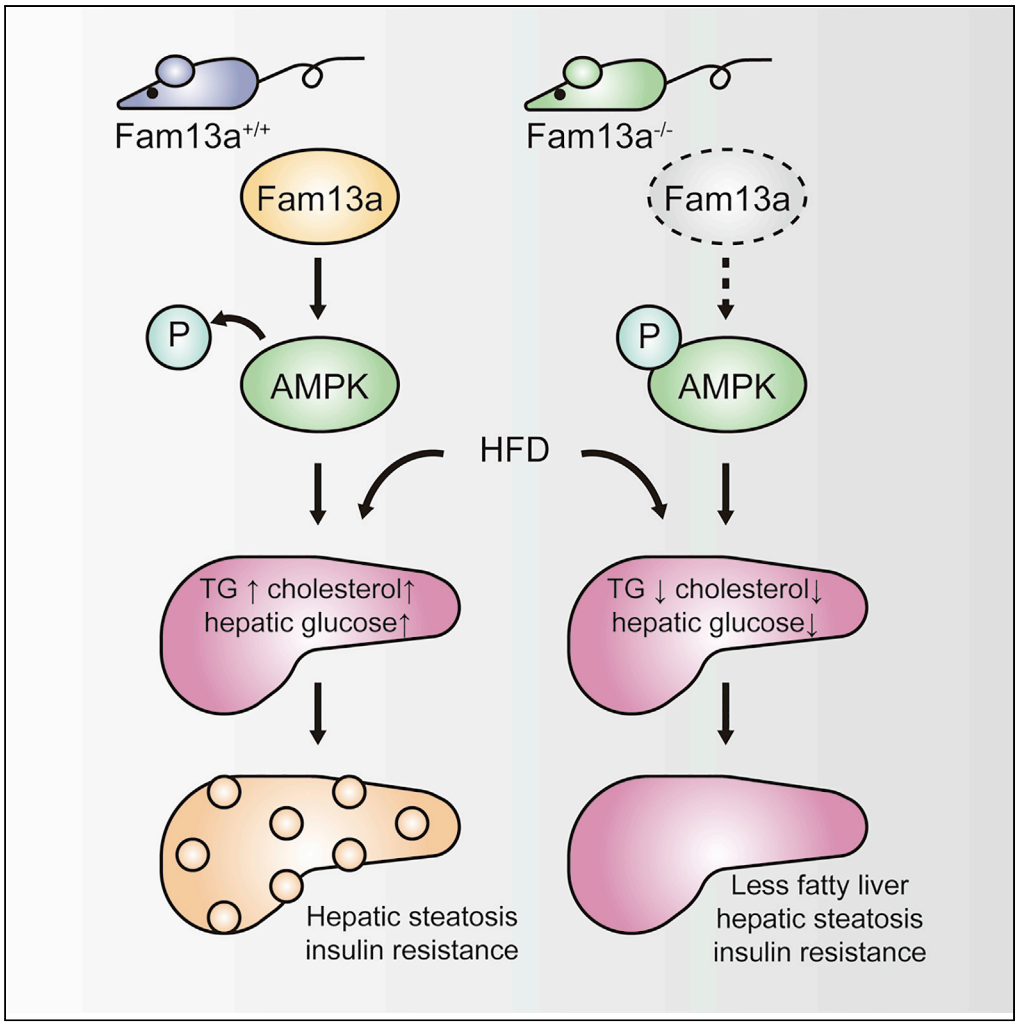

Xin Lin, Yae-Huei Liou, Yujun Li, ..., Guo Zhang, Chih-Hao Lee, Xiaobo Zhou

xlin7@bwh.harvard.edu (X.L.)
xiaobo.zhou@channing.harvard.edu (X.Z.)

HIGHLIGHTS

SNP rs2276936 regulates expression of endogenous FAM13A

Fam13a$^{-/-}$ mice are protected from high-fat-diet-induced obesity and fatty liver.

Fam13a$^{-/-}$ hepatocytes show increased mitochondrial respiration and AMPK activity

Lin et al., iScience *23*, 100928
March 27, 2020
https://doi.org/10.1016/j.isci.2020.100928

iScience

CellPress

Article

FAM13A Represses AMPK Activity and Regulates Hepatic Glucose and Lipid Metabolism

Xin Lin,[1,*] Yae-Huei Liou,[2] Yujun Li,[1,3] Lu Gong,[1] Yan Li,[1] Yuan Hao,[1] Betty Pham,[1] Shuang Xu,[1] Zhiqiang Jiang,[1] Lijia Li,[1] Yifan Peng,[4] Dandi Qiao,[1] Honghuang Lin,[5] Pengda Liu,[6] Wenyi Wei,[7] Guo Zhang,[8] Chih-Hao Lee,[2] and Xiaobo Zhou[1,9,*]

SUMMARY

Obesity commonly co-exists with fatty liver disease with increasing health burden worldwide. Family with Sequence Similarity 13, Member A (*FAM13A*) has been associated with lipid levels and fat mass by genome-wide association studies (GWAS). However, the function of FAM13A in maintaining metabolic homeostasis *in vivo* remains unclear. Here, we demonstrated that rs2276936 in this locus has allelic-enhancer activity in massively parallel reporter assays (MPRA) and reporter assay. The DNA region containing rs2276936 regulates expression of endogenous FAM13A in HepG2 cells. *In vivo*, *Fam13a*$^{-/-}$ mice are protected from high-fat diet (HFD)-induced fatty liver accompanied by increased insulin sensitivity and reduced glucose production in liver. Mechanistically, loss of Fam13a led to the activation of AMP-activated protein kinase (AMPK) and increased mitochondrial respiration in primary hepatocytes. These findings demonstrate that FAM13A mediates obesity-related dysregulation of lipid and glucose homeostasis. Targeting FAM13A might be a promising treatment of obesity and fatty liver disease.

INTRODUCTION

Incidence of obesity and nonalcoholic fatty liver disease (NAFLD) has been increasing rapidly and is now the most common cause of chronic liver diseases worldwide (Younossi, 2019; Younossi et al., 2018). NAFLD may develop into nonalcoholic steatohepatitis and increase the risk of cardiovascular diseases and mortality; however, efficient treatment to block or slow down progression of NAFLD is still lacking (Lefere et al., 2019; Younossi et al., 2018). Genome-wide association studies (GWAS) have been instrumental to pinpoint important susceptible genes and possible therapeutic targets (Cannon and Mohlke, 2018) in complex traits. Genetic variants in the FAM13A (Family with Sequence Similarity 13, Member A) locus has been reported to be associated with HDL cholesterol and body mass index (BMI)-adjusted fasting insulin levels (Lundback et al., 2018; Willer et al., 2013), two relevant phenotypes for liver diseases. Furthermore, FAM13A locus has also been identified for its significant association with waist-to-hip ratio (WHR) adjusted for body mass index (WHRadjBMI) (Shungin et al., 2015) and visceral to subcutaneous fat ratio (Ji et al., 2019).

Recently, FAM13A was reported to interact and stabilize IRS1 from degradation, thereby enhancing insulin signaling in adipocytes (Wardhana et al., 2018). In contrast, another group reported that Fam13a is dispensable for adipose development and insulin sensitivity in adipose tissue (Tang et al., 2019), suggesting complex regulation of glucose metabolism by FAM13A in adipose tissue. However, whether FAM13A regulates hepatic insulin sensitivity and lipid metabolism and their roles in fatty liver development are not explored yet.

In this study, we find that rs2276936 in the FAM13A locus, associated with multiple metabolic traits including HDL levels, demonstrated allelic enhancer activity. Furthermore, we find that *Fam13a*$^{-/-}$ mice showed improved hepatic insulin sensitivity and increased hepatic AMP-activated protein kinase (AMPK) activity, a major regulator in maintaining energy homeostasis and preventing against hepatic steatosis (Coughlan et al., 2014; Woods et al., 2017). These changes may collectively contribute to ameliorated high-fat diet (HFD)-induced obesity and nonalcoholic fatty liver in *Fam13a*$^{-/-}$ mice.

RESULTS

RS2276936 within FAM13A Gene Associated with HDL and Fat Mass Exerts Allelic Activity

Previously, we performed massively parallel reporter assays (MPRA) to assess allele-specific enhancer activity of SNPs within FAM13A GWAS locus (Castaldi et al., 2019) and identified 45 SNPs with significant

[1]Channing Division of Network Medicine, Department of Medicine, Brigham and Women's Hospital, Harvard Medical School, Boston, MA 02115, USA

[2]Department of Genetics and Complex Diseases, Harvard T.H. Chan School of Public Health, Boston, MA 02115, USA

[3]Guangzhou First People's Hospital, the Second Affiliated Hospital of South China University of Technology, Guangzhou, Guangdong 510180, China

[4]Department of Chemical and Biological Engineering, Tufts University, Boston, MA 02155, USA

[5]Section of Computational Biomedicine, Department of Medicine, Boston University School of Medicine, Boston, MA 02118, USA

[6]Lineberger Comprehensive Cancer Center and Department of Biochemistry and Biophysics, School of Medicine, The University of North Carolina, Chapel Hill, NC 27514, USA

[7]Department of Pathology, Beth Israel Deaconess Medical Center, Harvard Medical School, Boston, MA 02215, USA

[8]School of Public Health, Tongji Medical College, Huazhong University of Science and Technology, Wuhan, Hubei 430030, China

[9]Lead Contact

*Correspondence: xlin7@bwh.harvard.edu (X.L.), xiaobo.zhou@channing.harvard.edu (X.Z.)

https://doi.org/10.1016/j.isci.2020.100928

allelic effects. Given that the FAM13A locus associated with multiple metabolic traits including HDL levels, we further queried the association of these 45 MPRA SNPs with HDL levels using GWAS data from Global Lipids Genetics Consortium (Willer et al., 2013) (http://csg.sph.umich.edu/abecasis/public/lipids2013/). We found that three tightly correlated MPRA SNPs (r^2> 0.9) demonstrated genome-wide (rs2276936, $p < 10^{-8}$) or sub-genome-wide significance (rs2167750 and rs7695177, $p < 10^{-5}$) of association with HDL levels (Table S1). Furthermore, these three SNPs are tightly correlated with previously published top GWAS SNPs associated with lipid traits including rs3822072 (Yaghootkar et al., 2016) and rs9991328 (Yaghootkar et al., 2016) (r^2> 0.9 for all pairwise comparison). Major and minor haplotypes of these five SNPs comprised of >90% population of all ethnic groups (Machiela and Chanock, 2015, 2018) (Figure 1A). We also evaluated the association of these three SNPs, rs2276936, rs2167750, and rs7695177 with over 2000 complex traits from UK Biobank (Ge et al., 2017). They were associated with body fat distribution at genome-wide significance ($p < 5 \times 10^{-8}$) (Table S2).

Furthermore, we analyzed open chromatin status nearby three SNPs, rs2276936, rs2167750, and rs7695177 in primary human hepatic tissues and hepatocytes available from Roadmap epigenomics and ENCODE (encyclopedia of DNA elements) projects (Inoue et al., 2017; Kundaje et al., 2015). The DNA region nearby rs2276936 showed highest open chromatin scores among three SNPs, suggesting active regulatory element nearby this SNP in human liver tissues or cells (Figure 1B). To further investigate the regulatory effects of these three SNPs on the expression of FAM13A, we performed reporter assays by cloning the endogenous promoter of FAM13A gene and preceding SNP regions with one of two opposing alleles for each SNP into the luciferase constructs. The primers used for molecular cloning of reporter constructs are shown in Table S3. After transfection into HepG2 cells, rs2276936 demonstrated significant allelic effects (Figure 1B), with A-allele at forward orientation associated with higher luciferase activity. Furthermore, we engineered the CRISPR/Cas-9 constructs with either gRNA pairs to generate a ~100bp deletion (Figure 1C) or a single gRNA to generate an indel (Figure 1D) spanning rs2276936. Sequence of gRNAs used for deletion generation nearby the rs2276936 is shown in Table S4. After transfection of these CRISPR constructs into HepG2 cells, we found that deletion of rs2276936 region led to 30% reduction in the expression of FAM13A, suggesting an enhancer activity of the DNA region spanning rs2276936.

Collectively, these data strongly suggested rs2276936 associated with HDL-regulated expression of FAM13A in an allele-specific manner with rs2276936C allele associated with lower enhancer activity in HepG2 cells.

Fam13a Deficiency Ameliorates HFD-induced Body Weight Gain

Given that FAM13A was associated with multiple metabolic phenotypes in GWAS, we investigated metabolic phenotypes of Fam13a knockout mice that we have previously generated (Jiang et al., 2016). Consistent with the previous report, *Fam13a*$^{-/-}$ mice demonstrated similar body weights, serum-free fatty acid levels, and triglycerides levels as compared with wild-type littermate control mice (*Fam13a*$^{+/+}$) (Figures S1A–S1D) when fed on normal chow diet. However, total cholesterol levels are reduced in *Fam13a*$^{-/-}$ mice compared with *Fam13a*$^{+/+}$ (Figure S1E), suggesting that Fam13a is required to maintain normal cholesterol levels.

HFD-treated mice chronically develop multiple metabolic changes, seen in fatty liver disease, an increasing global health burden (Perlemuter et al., 2007). To determine roles of FAM13A in this process, we treated mice with HFD for four months. In contrast to *Fam13a*$^{+/+}$ mice, *Fam13a*$^{-/-}$ mice demonstrated less body weight gain starting at two months of HFD treatment (Figures 2A and S2A) and increased lean mass and reduced fat mass after four months of HFD feeding (Figures 2B and S2B), likely attributable to decreased mass of inguinal fat (Figures 2C and S2C) rather than brown or epididymal fat (Figures S2E–S2H). Furthermore, liver mass is also reduced in HFD-treated *Fam13a*$^{-/-}$ mice (Figures 2D and S2D). However, oxygen consumption (VO2) (Figures S3A and S3B), energy expenditure (EE) (Figure S3C), respiratory exchange rate (Figure S3D), and food intake (Figure S3E) were comparable in *Fam13a*$^{-/-}$ mice and *Fam13a*$^{+/+}$ mice after seven weeks of HFD treatment.

Fam13a$^{-/-}$ Mice Display Improved Hepatic Insulin Sensitivity and Reduced Hepatic Glucose Production

To assess glucose homeostasis, we performed glucose tolerance test (GTT) and insulin tolerance test (ITT) on *Fam13a*$^{-/-}$ mice and wild-type littermates after 14 weeks of HFD treatment. Despite similar fasting glucose levels (Figure S2I) and glucose tolerance (Figure 3A), *Fam13a*$^{-/-}$ mice demonstrated increased insulin sensitivity as suggested by ITT assay (Figure 3B), indicating that *Fam13a* deficiency sensitizes mice to

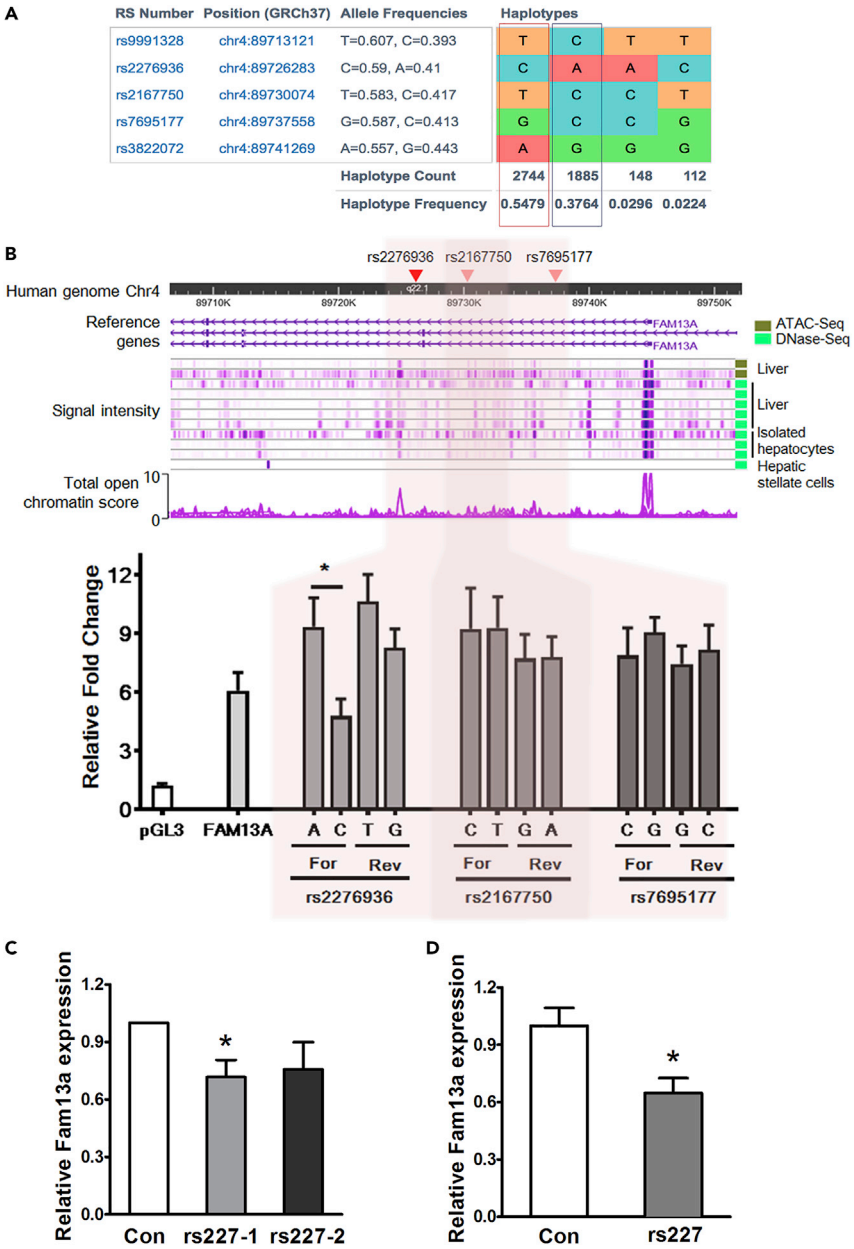

Figure 1. Identification of Functional Variants at the FAM13A Locus Associated with Lipid Levels

(A)LD matrix of SNPs (rs2276936, rs2167750, rs7695177) with previously frequently reported top GWAS SNPs (rs3822072 and rs9991328). The first two columns represent the major (red frame) and minor (blue frame) haplotypes of these five SNPs.

(B–D) (B) Top: the diagram shows the ATAC-Seq and DNase-Seq signals around SNP rs2276936, rs2167750, and rs7695177 in liver-relevant cell and tissues profiled by Roadmap epigenomics project and ENCODE project. Bottom: reporter assays of FAM13A promoter with or without DNA regions spanning rs2276936, rs2167750, and rs7695177 in HepG2 cells. For: forward orientation; Rev: reverse orientations. Data are presented as mean ± SEM from three biological replicates with triplicate wells in each repeat. *$p < 0.05$ by unpaired Student's t test. Expression of FAM13A was assessed in HepG2 cells transfected with gRNA targeting rs2276936 for regional deletion (C) or indel deletion (D). Con: Control. Rs227-1 and rs227-2 are from two independent repeats. Data are presented as mean ± SEM from two biological replicates with triplicate wells in each repeat. *$p < 0.05$ by unpaired Student's t test.

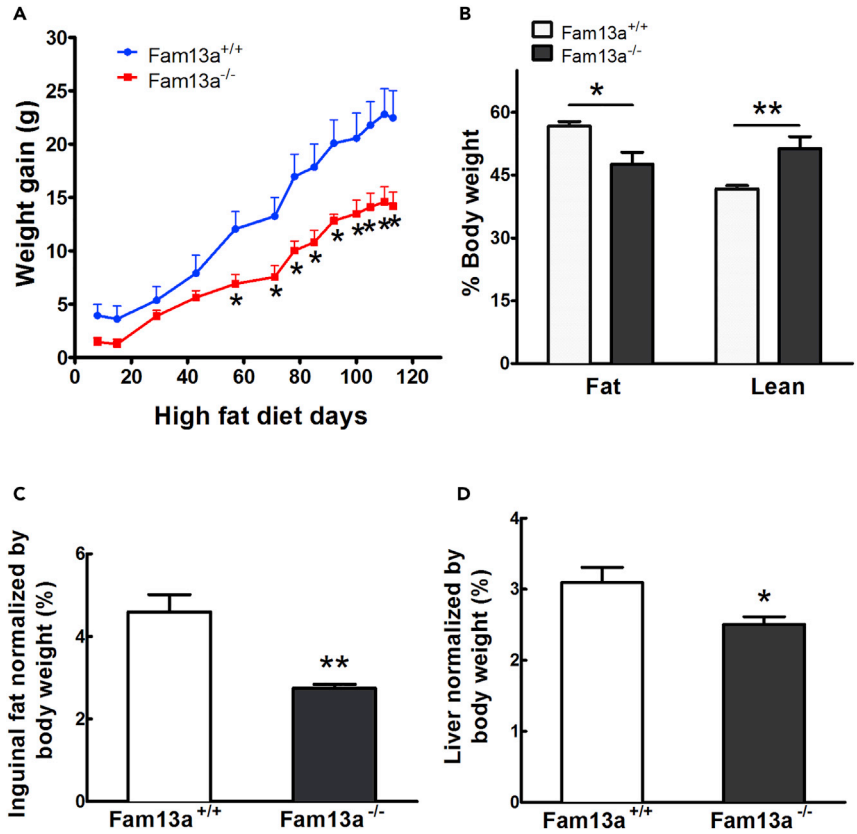

Figure 2. Body Weight Gain in Mice after High-Fat diet (HFD) Treatment for Four Months

(A) Gain of body weight measured during HFD treatment for four months in *Fam13a*$^{+/+}$ (n = 7) and *Fam13a*$^{-/-}$ mice (n = 5). (B–D) (B) Fat and lean mass of mice (A) measured by MRI after four months of HFD treatment. Inguinal fat (C) and liver (D) mass normalized to body weight in mice treated with HFD (n = 6 for *Fam13a*$^{+/+}$; n = 5 for *Fam13a*$^{-/-}$). Data are presented as mean ± SEM. *p < 0.05 or **p < 0.01 by unpaired Student's t test.

insulin response. However, we detected reduced insulin levels in serum from *Fam13a*$^{-/-}$ mice (Figure 3C), indicating a plausible feedback due to increased insulin sensitivity.

Because liver is critical in systemic glucose homeostasis, we analyzed hepatic insulin signaling pathway via portal vein injection of insulin into HFD-fed *Fam13a*$^{-/-}$ mice. Increased phosphorylation of Akt (p-Akt) (Thr308) was observed in *Fam13a*$^{-/-}$ mice compared with *Fam13a*$^{+/+}$ controls five minutes after insulin stimulation (Figure 3D). Furthermore, primary *Fam13a*$^{-/-}$ hepatocytes also demonstrated increased levels of p-Akt after insulin treatment *ex vivo* compared with *Fam13a*$^{+/+}$ cells (Figure 3E), suggesting increased hepatic insulin sensitivity in *Fam13a*$^{-/-}$ hepatocytes. Additionally, hepatic glucose production was also significantly decreased in isolated primary *Fam13a*$^{-/-}$ hepatocytes, compared with *Fam13a*$^{+/+}$ cells (Figure 3F), suggesting that deficiency of Fam13a may lead to intrinsic reduction of gluconeogenesis in hepatocytes.

Partially consistent with recent findings that Fam13a may increase IRS-1 levels in white adipose tissues (Wardhana et al., 2018), we found a trend toward reduced levels of IRS-1 in epididymal fat (Figure S4A) whereas slightly increased IRS-1 levels in both inguinal fat (Figure S4B) and liver tissues (Figure S4C) compared with *Fam13a*$^{+/+}$ control mice, suggesting that the regulation of Fam13a on insulin signaling in adipocytes is depot dependent.

FAM13A Regulates Lipid Metabolism and *Fam13a*$^{-/-}$ Mice Are Resistant to HFD-Induced Fatty Liver

Given that the FAM13A locus is associated with HDL levels in GWAS, we also measured lipid levels in HFD-fed mice. *Fam13a*$^{-/-}$ mice showed significantly reduced levels of LDL/VLDL and total cholesterol (Figure 4A) in

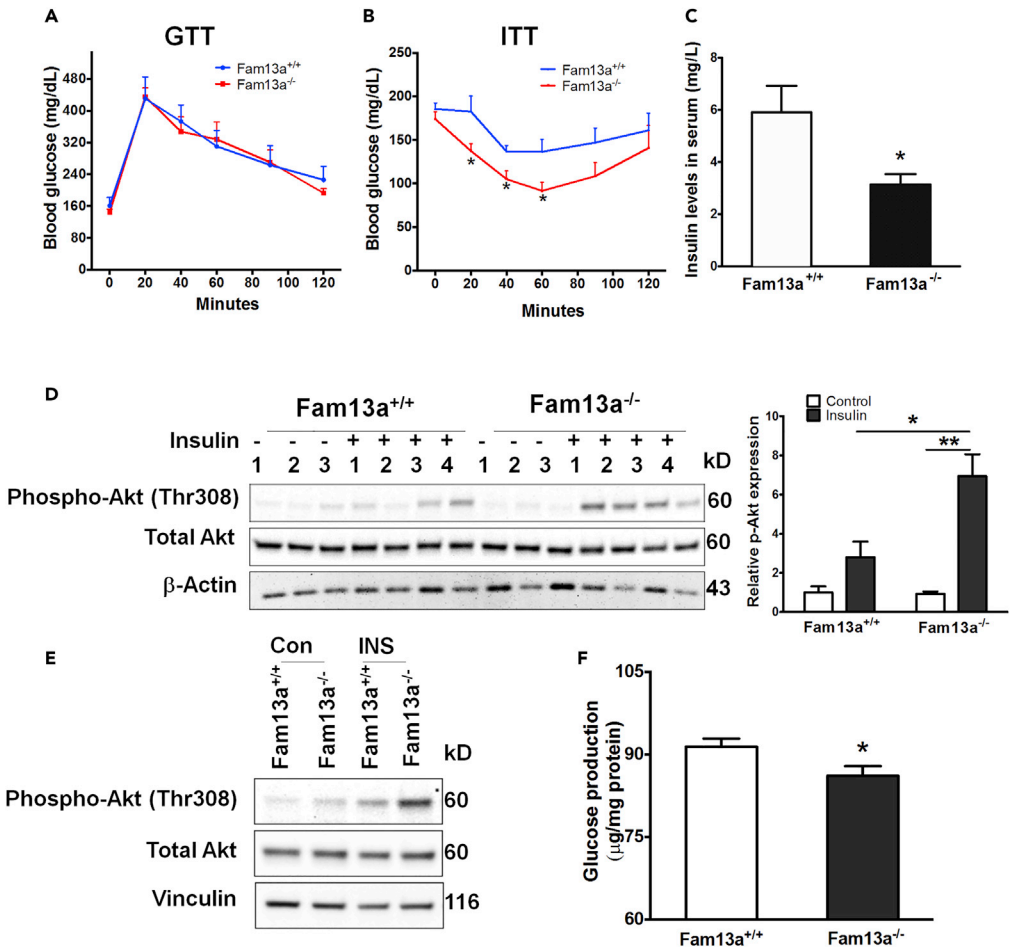

Figure 3. *Fam13a*$^{-/-}$ Mice Showed Improved Systemic and Hepatic Insulin Sensitivity after HFD Treatment

(A and B) (A) Glucose tolerance test (GTT) and (B) insulin tolerance test (ITT) were performed after overnight fasting or 6-h fasting in female *Fam13a*$^{+/+}$ and *Fam13a*$^{-/-}$ mice fed with HFD for 14 weeks, respectively.

(C) Serum insulin was measured in female *Fam13a*$^{+/+}$ and *Fam13a*$^{-/-}$ mice fed with HFD for four months.

(D) Immunoblotting of phosphorylation of Akt (Thr308) in liver from HFD-fed *Fam13a*$^{+/+}$ and *Fam13a*$^{-/-}$ mice for four months with or without insulin injection via portal vein. Mice were harvested five minutes after insulin treatment. Mean ± SEM shown represent the densitometry of bands averaged from 3 to 4 mice/group. *$p < 0.05$ or **$p < 0.01$ by unpaired Student's t test.

(E) Akt phosphorylation at Thr308 was measured in primary hepatocytes cultured in the presence or absence of insulin at the concentration of 100 nM for 6 h. INS, insulin.

(F) Hepatic glucose production was measured and normalized to total cellular protein amount in hepatocytes isolated from *Fam13a*$^{+/+}$ and *Fam13a*$^{-/-}$ mice. (Mean ± SEM from three mice/genotypes). *$p < 0.05$, unpaired Student's t test.

serum. Although levels of HDL (Figure 4A) and triglycerides (Figure S5A) in serum are comparable between *Fam13a*$^{-/-}$ and *Fam13a*$^{+/+}$ mice, expression of the apolipoprotein A-I (Apoa1) gene that encodes major component of HDL was significantly increased in isolated hepatocytes (Figure 4B) and showed a trend toward increased levels in liver samples (Figure S5B) from *Fam13a*$^{-/-}$ mice compared with *Fam13a*$^{+/+}$ littermates.

Chronic HFD treatment results in lipid accumulation in the liver, leading to fatty liver disease (Perlemuter et al., 2007). However, significantly lower levels of free fatty acid (Figure 4C), triglycerides (Figure 4D), and total cholesterol (Figure 4E) were detected in liver samples from *Fam13a*$^{-/-}$ mice compared with *Fam13a*$^{+/+}$ control mice fed with HFD. We observed much less lipid accumulation in the livers of *Fam13a*$^{-/-}$ mice as compared with HFD-fed *Fam13a*$^{+/+}$ mice (Figure 4F). Collectively, these data suggest that Fam13a deficiency ameliorates HFD-induced fatty liver. However, expression of inflammatory cytokines was comparable between these two genotypes (Figures S5C–S5I).

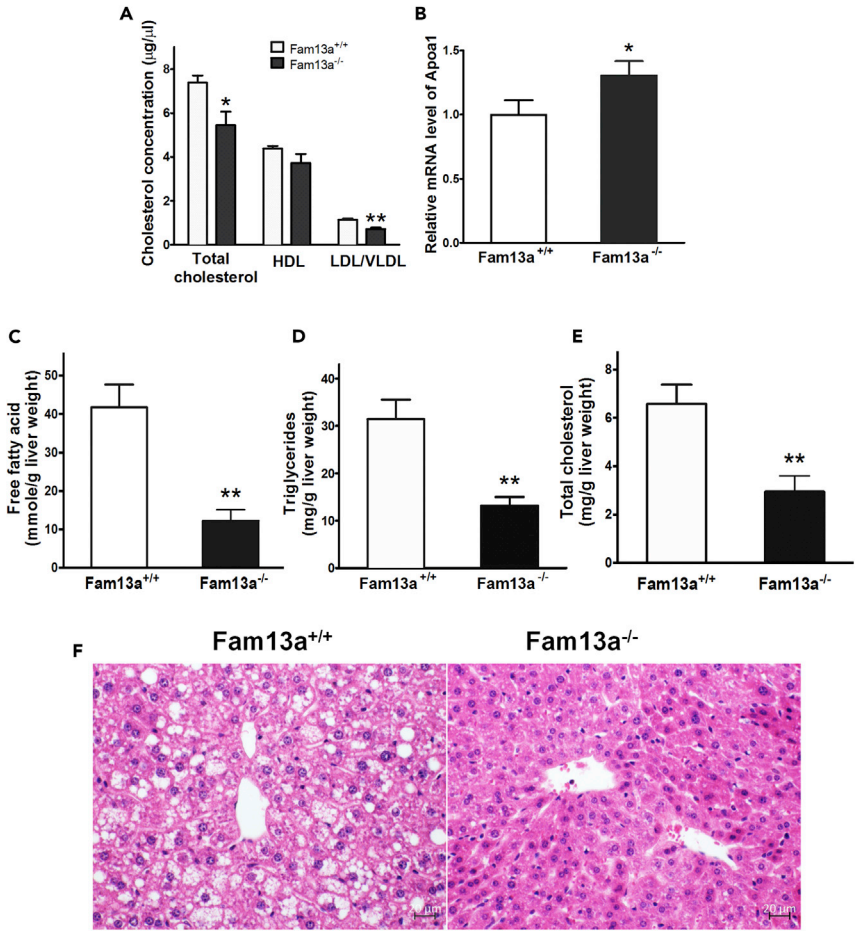

Figure 4. HFD-fed *Fam13a*$^{-/-}$ Mice Showed Improved Hepatic Steatosis

(A) Levels of total cholesterol, HDL, and LDL/VLDL were determined in serum from *Fam13a*$^{+/+}$ and *Fam13a*$^{-/-}$ mice after HFD treatment for four months.

(B–E) (B) Expression of Apoa1 was measured in primary hepatocytes from *Fam13a*$^{+/+}$ and *Fam13a*$^{-/-}$ mice using q-PCR. Free fatty acid (C), triglycerides (D), and cholesterol (E) were measured in murine liver samples. Data are presented as mean ± SEM. *$p < 0.05$ or **$p < 0.01$, unpaired Student's t test.

(F) Representative images of HE staining of livers are shown. (n = 6 for *Fam13a*$^{+/+}$; n = 5 for *Fam13a*$^{-/-}$ mice). Scale bar: 20 μm.

Increased Mitochondrial Function and Activation of the AMPK Signaling in Hepatocytes from *Fam13a*$^{-/-}$ Mice

To determine the mechanism for improved fatty liver in *Fam13a*$^{-/-}$ mice after HFD treatment, we assessed several possibilities including lipolysis, hepatic lipogenesis, mitochondrial function such as oxidative phosphorylation, and fatty acid oxidation in hepatocytes. First, lipolysis induced by injection of isoproterenol, a β3-adrenergic agonist, stimulated a significant increase of free fatty acid release in both *Fam13a*$^{+/+}$ and *Fam13a*$^{-/-}$ mice with negligible genotypic difference (Figure S6A). Secondly, expression of lipogenic genes including sterol regulatory element-binding transcription factor (Srebf1), a critical transcription factor to activate lipogenic gene (Hagiwara et al., 2012), and its target, fatty acid synthase (Fasn) (Radenne et al., 2008), were comparable in liver samples from *Fam13a*$^{-/-}$ and *Fam13*$^{+/+}$ mice (Figures S6B and S6C). Lastly, expression of critical genes for fatty acid β-oxidation, medium-chain acyl-coenzyme A dehydrogenase (Acadm), was increased in liver samples from HFD-fed *Fam13a*$^{-/-}$ mice (Figure S6D), in contrast to carnitinepalmitoyltransferase 1A (Cpt1a) (Figure S6E).

We then assessed mitochondrial function in primary hepatocytes. Indeed, basal and maximal mitochondrial respiration were significantly increased in *Fam13a*$^{-/-}$ hepatocytes, compared with *Fam13a*$^{+/+}$

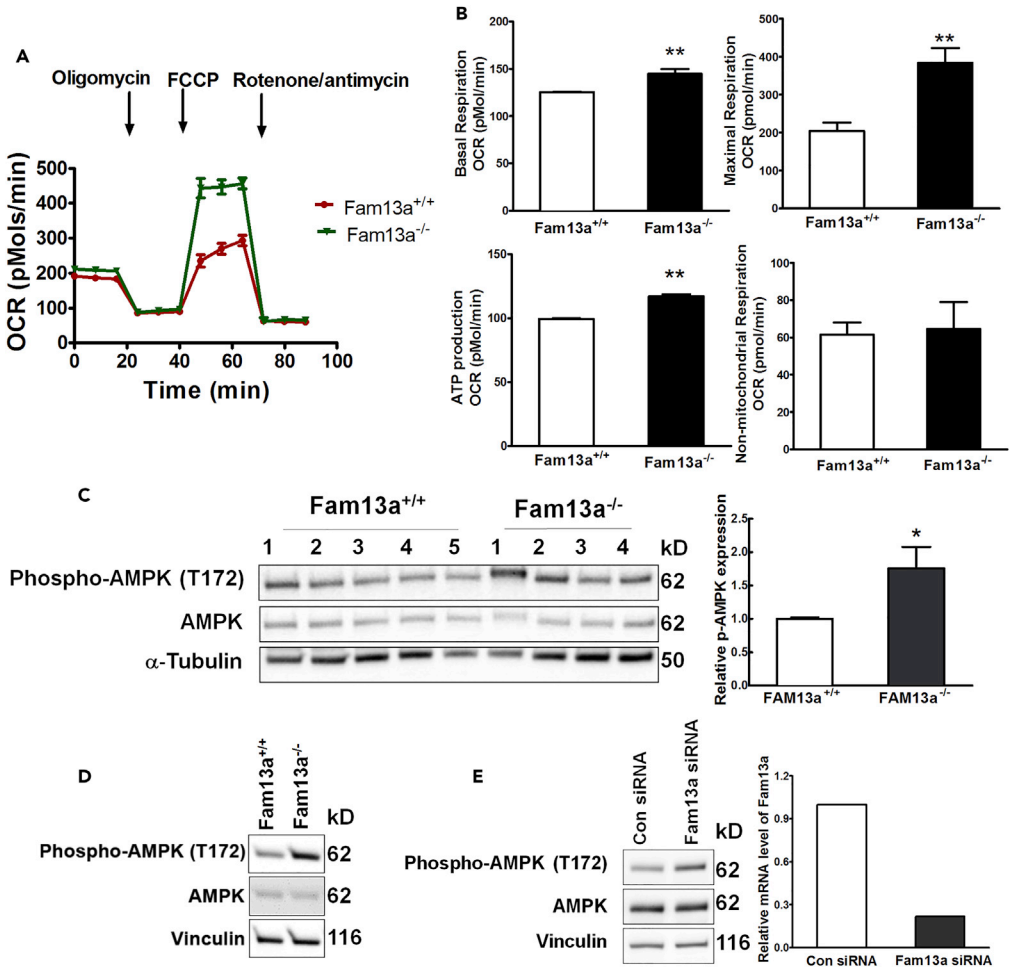

Figure 5. FAM13A Regulates Mitochondrial Function in Primary Hepatocytes

(A) Mitochondrial respiration was measured by Seahorse assay in hepatocytes isolated from *Fam13a*$^{+/+}$ and *Fam13a*$^{-/-}$ mice. Arrows indicate the sequential addition of oligomycin, carbonyl cyanide 4-(trifluoromethoxy) phenylhydrazone (FCCP), and rotenone/antimycin treatments. Representative results of one pair of mice from two biological replicates. (B–E) (B) The basal oxygen consumption rate (OCR), maximal mitochondrial respiration, ATP production, and non-mitochondrial respiration from A are shown. Data are presented as mean ± SD. **p < 0.01 by unpaired Student's t test. Phosphorylation of AMPK (Thr172) was measured in the liver samples from HFD-fed *Fam13a*$^{+/+}$ and *Fam13a*$^{-/-}$ mice (C, n = 4–5 mice/genotype), in primary hepatocytes (D) and HepG2 cells transfected with small interfering RNA (siRNA) targeting FAM13A (E). Data are presented as mean ± SEM. *p < 0.05, **p < 0.01 by unpaired Student's t test.

hepatocytes as measured by Seahorse assay (Figures 5A and 5B), suggesting increased mitochondrial oxidative phosphorylation in primary hepatocytes under Fam13a deficiency. Consistently, expression of peroxisome proliferative activated receptor, gamma, coactivator 1 alpha (Ppargc1α), the master regulator of mitochondrial biogenesis and oxidative phosphorylation (Jun et al., 2014), is increased in *Fam13a*$^{-/-}$ hepatocytes, compared with *Fam13a*$^{+/+}$ hepatocytes (Figure S6F).

Furthermore, we determined the activity of AMPK, a critical regulator in energy homeostasis, in *Fam13a*$^{-/-}$ liver samples. Accompanied by improved fatty liver in *Fam13a*$^{-/-}$ mice, AMPK activation as indicated by phosphorylation of AMPK (Thr172) was significantly enhanced in liver from *Fam13a*$^{-/-}$ mice fed with HFD (Figure 5C). Increased activation of AMPK was also detected in primary hepatocytes from *Fam13a*$^{-/-}$ mice fed on normal chow, suggesting an intrinsic inhibition on AMPK in hepatocytes by FAM13A (Figure 5D). This was further confirmed by increased AMPK activation detected in HepG2 cells transfected with FAM13A siRNA (Figure 5E). These data indicate that deficiency of *Fam13a* led to hepatic activation of AMPK pathway that may contribute to less body weight gain and ameliorated fatty liver in *Fam13a*$^{-/-}$ mice under HFD treatment.

FAM13A Regulates Mitochondrial Function through AMPK Signaling

Furthermore, overexpression of FAM13A reduced basal and maximal mitochondrial respiration, and ATP production (Figure 6A), accompanied by decreased phosphorylation level of AMPK (Thr172) (Figure 6B) in HepG2 cells. To determine whether FAM13A regulates mitochondrial function through AMPK, stable knockdown of AMPK or FAM13A was established in HepG2 cells by shRNA targeting AMPKα and/or FAM13A, as opposed to scramble RNA control. Although knockdown of FAM13A led to increased mitochondrial respiration (Figures 6C–6E), this was abolished by silencing of AMPK. Taken together, these data suggest that FAM13A regulates mitochondrial function through dephosphorylation and inactivation of AMPK and thus possibly promotes lipid accumulation in hepatic cells (Figure 7A).

DISCUSSION

Our current studies provided *in vivo* and *in vitro* evidence supporting important roles of FAM13A, a gene consistently associated with multiple metabolic phenotypes in GWAS, in regulating hepatic glucose and lipid metabolism. By reporter and CRISPR/Cas-9 assays, we pinpointed rs2276936 as the possible functional variant regulating hepatic FAM13A expression. Furthermore, we demonstrated that *Fam13a*$^{-/-}$ mice are protected from HFD-induced fatty liver and lipid toxicity with improved hepatic insulin sensitivity. Increased AMPK activation associated with increased mitochondrial respiration was detected in hepatocytes from *Fam13a*$^{-/-}$ mice, which likely contributes to ameliorated HFD-induced fatty liver in *Fam13a*$^{-/-}$ mice. Importantly, most of the directional effects of risk allele rs2276936C were recapitulated in knockout mouse model, such as fat mass, insulin sensitivity, and total cholesterol levels (Figure 7B). Admittedly, some of human GWAS traits were not confirmed with genotypic difference in mouse models such as HDL levels, further highlighting the complexity of using mouse model to recapitulate human GWAS findings (Small et al., 2018).

From GWAS to Function

Identification of functional variants in the GWAS locus is the crucial and necessary first step to translate genetic discoveries to disease understanding and ultimately, therapy. The FAM13A locus has been associated with BMI-adjusted fasting insulin level (Lundback et al., 2018), HDL level (Willer et al., 2013), and waist-to-hip ratio (Shungin et al., 2015) in GWAS in multiple replicated studies. However, functional variants in this region and function of FAM13A gene in regulating metabolism *in vivo* remain incompletely understood yet. Here, we identified rs2276936 with allelic enhancer activities is located in the first intron of FAM13A, about ~18kb away from its transcription start site. Interestingly, this SNP is also located nearby multiple enhancer marks including H3K4Me1, H3K27Ac, and H3K9Ac as well as DNase hypersensitive sites in liver, suggesting regulatory function of rs2276936. We primarily focused on roles of rs2276936 in liver here, given the importance of liver in regulating HDL, lipid, and glucose metabolism. Further investigations are warranted to determine roles of rs2276936 in adipose tissue and other metabolic active tissues. It is not surprising that pleiotropic functional variants may have effects on multiple tissues. For example, the significant BMI GWAS SNPs in the fat mass and obesity-associated (FTO) locus may regulate Iroquois homeobox 3 (Irx3) and Iroquois homeobox 5 (Irx5), the major causal genes (Smemo et al., 2014), in both brain (Smemo et al., 2014) and adipose tissues (Claussnitzer et al., 2015). Functional variants regulating lipid GWAS gene sortilin 1 (Sort1) demonstrated greater allelic effects in the liver sample (Musunuru et al., 2010) despite abundant expression of Sort1 in adipose tissues. These examples highlight the challenges and complexity of functional variants identification in GWAS loci in effect cell types.

It is noteworthy that rs2276936C, tightly correlated with previous top GWAS SNP rs9991328T (Figure 1A), is associated with reduced fat mass in human subjects (Table S2) and reduced enhancer activity for Fam13A (Figure 1B), which is consistent with reduced body and fat weight in *Fam13a*$^{-/-}$ *mice* (Figures 2A and 2C) in mouse models as we summarized in Figure 7.

Insulin Sensitivity in *Fam13a*$^{-/-}$ Mice

Through ITT measurements, we observed increased insulin sensitivity in *Fam13a*$^{-/-}$ mice than *Fam13a*$^{+/+}$ mice fed with HFD. However, no glucose tolerance difference was detected by GTT assay. This may result from compensatory reduction of insulin levels in *Fam13a*$^{-/-}$ mice (Figure 3C).

Hepatic glucose production is also crucial for maintaining glucose homeostasis that is mainly controlled by gluconeogenesis through insulin and glucagon pathways. Reduced hepatic glucose production may result

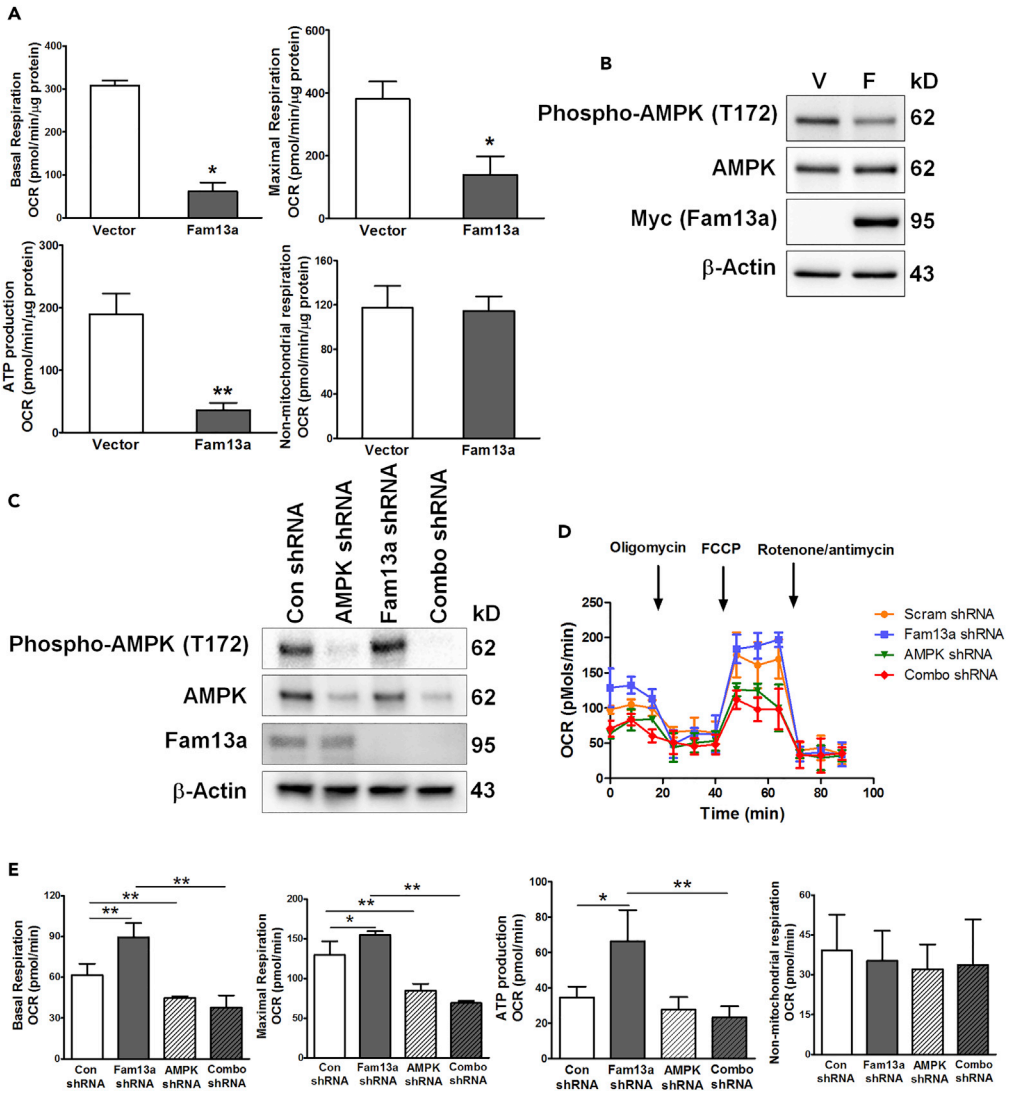

Figure 6. FAM13A Regulates Mitochondrial Respiration through AMPK Signaling

(A) The basal mitochondrial respiration, maximal mitochondrial respiration, ATP production, and non-mitochondrial respiration were shown in HepG2 cells transfected with the plasmid expressing FAM13A or empty vector. Data are presented as mean ± SEM. *$p < 0.05$, **$p < 0.01$ by unpaired Student's t test.

(B) Phosphorylation of AMPK (Thr172) was determined in HepG2 cells with overexpression of Myc-tagged FAM13A. V: Vector control; F: Fam13a.

(C) Immunoblotting showing the knockdown efficiency. Combo shRNA: combination of FAM13A shRNA and AMPK shRNA.

(D) Bioenergetics assays measured by Seahorse in HepG2 cells with stable knockdown of FAM13A and/or AMPK by shRNA. Arrows indicated sequential addition of oligomycin, carbonyl cyanide 4-(trifluoromethoxy) phenylhydrazone (FCCP), and rotenone/antimycin.

(E) The basal oxygen consumption rate (OCR), maximal mitochondrial respiration, ATP production, and non-mitochondrial respiration were shown. Data are presented as mean ± SD. *$p < 0.05$, **$p < 0.01$ by unpaired Student's t test.

from increased insulin sensitivity in *Fam13a*$^{-/-}$ hepatocytes through inhibition on the gluconeogenesis by insulin. Given that increased insulin sensitivity upon Fam13a deficiency was detected in primary hepatocytes isolated from normal chow- and HFD-fed mice, FAM13A likely intrinsically inhibits hepatic insulin sensitivity.

In contrast, the regulation of FAM13A on insulin sensitivity in adipose tissues seems more complex depending on the depots of white adipose tissue, which may explain previously inconsistent results

A

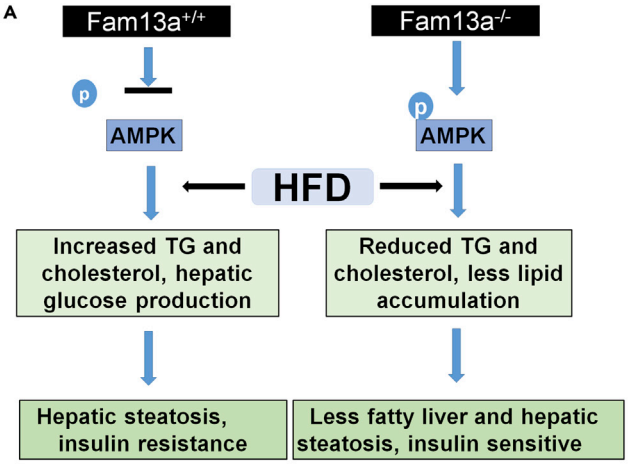

B

Species	Genotype	Fam13a expression	Fat mass	Insulin sensitivity	HDL
Human	rs2276936A	↑	↑	↓	↓
	rs2276936C	↓	↓	↑	↑
Mouse	Fam13a$^{-/-}$	↓	↓	↑	-

Figure 7. Schematic Illustration of FAM13A Regulating lipid and Glucose Metabolism

(A) Mechanism of FAM13A regulating Hepatic steatosis and insulin resistance through AMPK. TG: triglycerides. HFD: high-fat diet.

(B) Metabolic phenotypes observed in human subjects with opposing genotypes for SNP rs2276936 and *Fam13a*$^{-/-}$ mice (Ji et al., 2019).

ranging from reduced (Wardhana et al., 2018) to similar (Tang et al., 2019) insulin sensitivity in adipose tissues from *Fam13a*$^{-/-}$ mice fed with HFD. We found variable changes of IRS-1 in different types of adipose tissues from *Fam13a*$^{-/-}$ mice with a trend toward decreased levels of IRS-1 in epididymal fat (Figure S4A), similar as previously reported (Wardhana et al., 2018), whereas slightly increased IRS-1 levels in inguinal fat (Figure S4B).

Other reasons for some of the discrepancies between two previous studies and ours may include differences in the composition of diet, HFD treatment age and duration, genetic backgrounds of *Fam13a*$^{-/-}$ mice, and technical details, which may complicate results interpretation. For example, an HFD containing 35% fat, 25.3% carbohydrates, and 23% protein was used previously to feed six-week-old *Fam13a*$^{-/-}$ mice (C57BL/6N background) for 14 weeks compared with wild-type C57BL/6N mice in the studies (Wardhana et al., 2018). Herein, four- to five-month-old *Fam13a*$^{-/-}$ mice after three generations of backcrossing toward C57BL/6J background and *Fam13a*$^{+/+}$ littermates were fed with HFD containing 36% fat, 35.7% carbohydrates, and 20.5% protein for four months. Furthermore, previous ITT assay was performed in mice without fasting (Wardhana et al., 2018), in contrast to our ITT assay with mice after 6 h of fasting. Therefore, experimental condition is critical to interpret metabolic phenotypes in mice, and more stringently controlled studies are required to elucidate how FAM13A modulates insulin sensitivity in the adipose tissue.

Ameliorated Fatty Liver and Increased AMPK Activation in the *Fam13a*$^{-/-}$ Mice

Insulin sensitivity, body weight gain, and fatty liver can influence each other. Reduced body weight can possibly improve fatty liver and insulin resistance, whereas HFD-induced hepatic insulin resistance may lead to fatty liver due to failed inhibition on gluconeogenesis combined with selectively enhanced lipogenesis in liver by insulin (Petersen et al., 2017). In the present study, given reduced gluconeogenesis was found

in isolated primary hepatocytes from *Fam13a*$^{-/-}$ mice, it is likely ameliorated fatty liver resulted from improved hepatic insulin sensitivity. Furthermore, in HFD-fed *Fam13a*$^{-/-}$ mice, despite increased hepatic insulin sensitivity, improved fatty liver was found without significantly increased lipogenesis by insulin pathway, possibly due to hepatic activation of AMPK. Admittedly, future studies using liver-specific *Fam13a*$^{-/-}$ mice will be helpful to conclusively exclude the possibility of improved fatty liver resulting from less body weight gain in *Fam13a*$^{-/-}$ mice.

AMPK is activated by reduced ATP/AMP ratio due to prolonged energy deprivation, thus facilitating utilization of various sources of nutrients to generate ATP. Consequently, upon AMPK activation, ATP-consuming pathways, including cholesterol and fatty acid synthesis, are repressed and ATP-generating pathways, including fatty acid oxidation and lipolysis, are activated (Woods et al., 2017) through regulatory enzymes or regulatory proteins involved in anabolic pathways (Hardie et al., 2012). For example, AMPK represses cholesterol synthesis by inhibiting sterol regulatory element-binding factor 2 (Srebf2) and hydroxymethylglutaryl-CoA (HMG-CoA) reductase (Li et al., 2011). Therefore, activation of AMPK in primary hepatocytes isolated from *Fam13a*$^{-/-}$ mice may explain reduced cholesterol levels in serum from *Fam13a*$^{-/-}$ mice fed with normal chow (Figure S1E). Furthermore, increased mitochondrial respiration in primary *Fam13a*$^{-/-}$ hepatocytes is also consistent with enhanced expression of Ppargc1α, a key gene essential for mitochondrial synthesis and regulated by AMPK (Hardie et al., 2012).

AMPK was recently suggested as a therapeutic target for the treatment of obesity, fatty liver disease (Garcia et al., 2019), and type 2 diabetes (Coughlan et al., 2014) due to its importance as a master regulator in maintaining glucose and lipid homeostasis. For example, genetic or pharmacological activation of AMPK in murine livers decreased lipogenesis, ameliorated high-fructose-induced hepatic triglyceride accumulation and thus improved hepatic steatosis (Woods et al., 2017), similar as we observed in HFD-fed *Fam13a*$^{-/-}$ mice. Notably, hepatic activation of AMPK by overexpression of trancated AMPKα1 induced by doxycycline treatment improved HFD-induced weight gain and white fat depot accumulation, even after obesity and fatty liver disease have been established (Garcia et al., 2019). In addition, such hepatic activation of AMPK usually does not reduce levels of blood glucose (Cokorinos et al., 2017; Woods et al., 2017), as we observed as well (Figure S2I). Admittedly, hepatic role of AMPK activation in regulating body weight gain is far more complex. Despite knockin of activating mutations in the AMPKγ2 subunit reduced fat mass and liver steatosis upon diet-induced obesity (Yang et al., 2016), liver-specific constitutive activation of AMPK protected mice against only high-fructose diet-induced liver steatosis (Woods et al., 2017), in contrast to HFD treatment.

It is likely that hepatic activation of AMPK pathway may not explain all the metabolic phenotypes that we observed in *Fam13a*$^{-/-}$ mice, and future studies using hepatocyte-specific and/or adipocyte-specific Fam13a knockout mice may help explain the pleotrophic regulation of FAM13A on glucose and lipid metabolism. Nonetheless, our study provides several lines of evidence to reveal that a common DNA variant rs2276936 associated with four metabolic traits regulates hepatic expression of FAM13A. *Fam13a*$^{-/-}$ mice are protected from HFD-induced weight gain, hepatic lipid accumulation, and insulin resistance, possibly by increasing the AMPK activity. More importantly, in human subjects, FAM13A locus is associated with lipid metaoblism and insulin sensitivity and increased expression of FAM13A was found in liver cirrhosis tissues compared with normal liver samples (Zhang et al., 2019). Given protective effects of Fam13a deficiency in diet-induced fatty liver, our results suggest FAM13A as a possible interventional target for the treatment of obesity and fatty liver disease.

Limitations of the Study

We demonstrated that deficiency of FAM13A protected mice from HFD-induced obesity and fatty liver using a global Fam13a knockout mouse line. To conclusively determine whether FAM13A deficiency in liver or fat contributes to amolriated body weight gain and lipid accumulation in liver after HFD treatment, future studies with hepatocyte-specific *Fam13a*$^{-/-}$ mice and adipose-specific *Fam13a*$^{-/-}$ mice are warranted. Secondly, despite phosphorylation of AMPK at Thr172 has been widely used to indicate AMPK activity, future more compreheisve evalautation on AMPK acitivty measured by AMPK activity kits including tissue-speicific regulation of AMPK by FAM13A would strengthen our findings. Lastly, future work will also include testing the silencing of Fam13a as a possible treatment strategy in diet-induced obesity and fatty liver mouse models.

METHODS

All methods can be found in the accompanying Transparent Methods supplemental file.

SUPPLEMENTAL INFORMATION

Supplemental Information can be found online at https://doi.org/10.1016/j.isci.2020.100928.

ACKNOWLEDGEMENTS

This work was supported by National Institutes of Health (NIH) grants: R01HL127200, R01HL137927 and R33 HL120794 to X. Z. and R01DK113791 and R21AI131659 to C.H.L.

AUTHOR CONTRIBUTIONS

X.Z., C.H.L., and X.L. designed the study. Y.L., X.L., and L.G. performed Seahorse assay. X.L., X.Z., and G.Z. performed data analysis. X.L., Y.L., and Y.P. did Western blot and Immunoprecipitation. X.L. and S.X. performed and analyzed animal experiments. Y.H.L. and X.L. isolated primary hepatocytes and performed cell experiments in primary hepatocytes. W.W. and Z.J. provided plasmids. B.P., Y.H., Y.L., and L.L. performed real-time PCR. X.L., X.Z., P.L., W.W., G.Z., and C.H.L. wrote the manuscript.

DECLARATION OF INTERESTS

The authors declare no competing interests.

Received: January 15, 2020
Revised: February 12, 2020
Accepted: February 17, 2020
Published: March 27, 2020

REFERENCES

Cannon, M.E., and Mohlke, K.L. (2018). Deciphering the emerging complexities of molecular mechanisms at GWAS loci. Am. J. Hum. Genet. *103*, 637–653.

Castaldi, P.J., Guo, F., Qiao, D., Du, F., Naing, Z.Z.C., Li, Y., Pham, B., Mikkelsen, T.S., Cho, M.H., Silverman, E.K., et al. (2019). Identification of functional variants in the FAM13A chronic obstructive pulmonary disease genome-wide association study locus by massively parallel reporter assays. Am. J.Respir.Crit. Care Med. *199*, 52–61.

Claussnitzer, M., Dankel, S.N., Kim, K.H., Quon, G., Meuleman, W., Haugen, C., Glunk, V., Sousa, I.S., Beaudry, J.L., Puviindran, V., et al. (2015). FTO obesity variant circuitry and adipocyte browning in humans. N. Engl. J. Med. *373*, 895–907.

Cokorinos, E.C., Delmore, J., Reyes, A.R., Albuquerque, B., Kjobsted, R., Jorgensen, N.O., Tran, J.L., Jatkar, A., Cialdea, K., Esquejo, R.M., et al. (2017). Activation of skeletal muscle AMPK promotes glucose disposal and glucose lowering in non-human primates and mice. Cell Metab. *25*, 1147–1159.e10.

Coughlan, K.A., Valentine, R.J., Ruderman, N.B., and Saha, A.K. (2014). AMPK activation: a therapeutic target for type 2 diabetes? Diabetes Metab. Syndr. Obes. *7*, 241–253.

Garcia, D., Hellberg, K., Chaix, A., Wallace, M., Herzig, S., Badur, M.G., Lin, T., Shokhirev, M.N., Pinto, A.F.M., Ross, D.S., et al. (2019). Genetic liver-specific AMPK activation protects against diet-induced obesity and NAFLD. Cell Rep. *26*, 192–208.e196.

Ge, T., Chen, C.Y., Neale, B.M., Sabuncu, M.R., and Smoller, J.W. (2017). Phenome-wide heritability analysis of the UK Biobank. PLoS Genet. *13*, e1006711.

Hagiwara, A., Cornu, M., Cybulski, N., Polak, P., Betz, C., Trapani, F., Terracciano, L., Heim, M.H., Ruegg, M.A., and Hall, M.N. (2012). Hepatic mTORC2 activates glycolysis and lipogenesis through Akt, glucokinase, and SREBP1c. Cell Metab. *15*, 725–738.

Hardie, D.G., Ross, F.A., and Hawley, S.A. (2012). AMPK: a nutrient and energy sensor that maintains energy homeostasis. Nat. Rev. Mol. Cell Biol. *13*, 251–262.

Inoue, F., Kircher, M., Martin, B., Cooper, G.M., Witten, D.M., McManus, M.T., Ahituv, N., and Shendure, J. (2017). A systematic comparison reveals substantial differences in chromosomal versus episomal encoding of enhancer activity. Genome Res. *27*, 38–52.

Ji, Y., Yiorkas, A.M., Frau, F., Mook-Kanamori, D., Staiger, H., Thomas, E.L., Atabaki-Pasdar, N., Campbell, A., Tyrrell, J., Jones, S.E., et al. (2019). Genome-wide and abdominal MRI data provide evidence that a genetically determined favorable adiposity phenotype is characterized by lower ectopic liver fat and lower risk of type 2 diabetes, heart disease, and hypertension. Diabetes *68*, 207–219.

Jiang, Z., Lao, T., Qiu, W., Polverino, F., Gupta, K., Guo, F., Mancini, J.D., Naing, Z.Z., Cho, M.H., Castaldi, P.J., et al. (2016). A chronic obstructive pulmonary disease susceptibility gene, FAM13A, regulates protein stability of beta-catenin. Am. J. Respir. Crit. Care Med. *194*, 185–197.

Jun, H.J., Joshi, Y., Patil, Y., Noland, R.C., and Chang, J.S. (2014). NT-PGC-1alpha activation attenuates high-fat diet-induced obesity by enhancing brown fat thermogenesis and adipose tissue oxidative metabolism. Diabetes *63*, 3615–3625.

Kundaje, A., Meuleman, W., Ernst, J., Bilenky, M., Yen, A., Heravi-Moussavi, A., Kheradpour, P., Zhang, Z., Wang, J., Ziller, M.J., et al. (2015). Integrative analysis of 111 reference human epigenomes. Nature *518*, 317–330.

Lefere, S., Van de Velde, F., Hoorens, A., Raevens, S., Van Campenhout, S., Vandierendonck, A., Neyt, S., Vandeghinste, B., Vanhove, C., Debbaut, C., et al. (2019). Angiopoietin-2 promotes pathological angiogenesis and is a therapeutic target in murine nonalcoholic fatty liver disease. Hepatology *69*, 1087–1104.

Li, Y., Xu, S., Mihaylova, M.M., Zheng, B., Hou, X., Jiang, B., Park, O., Luo, Z., Lefai, E., Shyy, J.Y., et al. (2011). AMPK phosphorylates and inhibits SREBP activity to attenuate hepatic steatosis and atherosclerosis in diet-induced insulin-resistant mice. Cell Metab. *13*, 376–388.

Lundback, V., Kulyte, A., Strawbridge, R.J., Ryden, M., Arner, P., Marcus, C., and Dahlman, I. (2018). FAM13A and POM121C are candidate genes for fasting insulin: functional follow-up analysis of a genome-wide association study. Diabetologia *61*, 1112–1123.

Machiela, M.J., and Chanock, S.J. (2015). LDlink: a web-based application for exploring population-specific haplotype structure and linking correlated alleles of possible functional variants. Bioinformatics *31*, 3555–3557.

Machiela, M.J., and Chanock, S.J. (2018). LDassoc: an online tool for interactively exploring genome-wide association study results and prioritizing variants for functional investigation. Bioinformatics *34*, 887–889.

Musunuru, K., Strong, A., Frank-Kamenetsky, M., Lee, N.E., Ahfeldt, T., Sachs, K.V., Li, X., Li, H., Kuperwasser, N., Ruda, V.M., et al. (2010). From noncoding variant to phenotype via SORT1 at the 1p13 cholesterol locus. Nature *466*, 714–719.

Perlemuter, G., Bigorgne, A., Cassard-Doulcier, A.M., and Naveau, S. (2007). Nonalcoholic fatty liver disease: from pathogenesis to patient care. Nat. Clin. Pract. Endocrinol. Metab. *3*, 458–469.

Petersen, M.C., Vatner, D.F., and Shulman, G.I. (2017). Regulation of hepatic glucose metabolism in health and disease. Nat. Rev. Endocrinol. *13*, 572–587.

Radenne, A., Akpa, M., Martel, C., Sawadogo, S., Mauvoisin, D., and Mounier, C. (2008). Hepatic regulation of fatty acid synthase by insulin and T3: evidence for T3 genomic and nongenomic actions. Am. J. Physiol. Endocrinol. Metab. *295*, E884–E894.

Shungin, D., Winkler, T.W., Croteau-Chonka, D.C., Ferreira, T., Locke, A.E., Magi, R., Strawbridge, R.J., Pers, T.H., Fischer, K., Justice, A.E., et al. (2015). New genetic loci link adipose and insulin biology to body fat distribution. Nature *518*, 187–196.

Small, K.S., Todorcevic, M., Civelek, M., El-SayedMoustafa, J.S., Wang, X., Simon, M.M., Fernandez-Tajes, J., Mahajan, A., Horikoshi, M., Hugill, A., et al. (2018). Regulatory variants at KLF14 influence type 2 diabetes risk via a female-specific effect on adipocyte size and body composition. Nat. Genet. *50*, 572–580.

Smemo, S., Tena, J.J., Kim, K.H., Gamazon, E.R., Sakabe, N.J., Gomez-Marin, C., Aneas, I., Credidio, F.L., Sobreira, D.R., Wasserman, N.F., et al. (2014). Obesity-associated variants within FTO form long-range functional connections with IRX3. Nature *507*, 371–375.

Tang, J., Zhou, H., Sahay, K., Xu, W., Yang, J., Zhang, W., and Chen, W. (2019). Obesity-associated family with sequence similarity 13, member A (FAM13A) is dispensable for adipose development and insulin sensitivity. Int. J. Obes.(Lond.) *43*, 1269–1280.

Wardhana, D.A., Ikeda, K., Barinda, A.J., Nugroho, D.B., Qurania, K.R., Yagi, K., Miyata, K., Oike, Y., Hirata, K.I., and Emoto, N. (2018). Family with sequence similarity 13, member A modulates adipocyte insulin signaling and preserves systemic metabolic homeostasis. Proc.Natl.Acad.Sci. U S A *115*, 1529–1534.

Willer, C.J., Schmidt, E.M., Sengupta, S., Peloso, G.M., Gustafsson, S., Kanoni, S., Ganna, A., Chen, J., Buchkovich, M.L., Mora, S., et al. (2013). Discovery and refinement of loci associated with lipid levels. Nat. Genet. *45*, 1274–1283.

Woods, A., Williams, J.R., Muckett, P.J., Mayer, F.V., Liljevald, M., Bohlooly, Y.M., and Carling, D. (2017). Liver-specific activation of AMPK prevents steatosis on a high-fructose diet. Cell Rep. *18*, 3043–3051.

Yaghootkar, H., Lotta, L.A., Tyrrell, J., Smit, R.A., Jones, S.E., Donnelly, L., Beaumont, R., Campbell, A., Tuke, M.A., Hayward, C., et al. (2016). Genetic evidence for a link between favorable adiposity and lower risk of type 2 diabetes, hypertension, and heart disease. Diabetes *65*, 2448–2460.

Yang, X., Mudgett, J., Bou-About, G., Champy, M.F., Jacobs, H., Monassier, L., Pavlovic, G., Sorg, T., Herault, Y., Petit-Demouliere, B., et al. (2016). Physiological expression of AMPKgamma2RG mutation causes Wolff-Parkinson-white syndrome and induces kidney injury in mice. J. Biol. Chem. *291*, 23428–23439.

Younossi, Z.M. (2019). Non-alcoholic fatty liver disease - a global public health perspective. J. Hepatol. *70*, 531–544.

Younossi, Z.M., Loomba, R., Rinella, M.E., Bugianesi, E., Marchesini, G., Neuschwander-Tetri, B.A., Serfaty, L., Negro, F., Caldwell, S.H., Ratziu, V., et al. (2018). Current and future therapeutic regimens for nonalcoholic fatty liver disease and nonalcoholic steatohepatitis. Hepatology *68*, 361–371.

Zhang, Y., Wang, S., Wang, C., Xiao, J., Zhang, S., and Zhou, H. (2019). High expression of FAM13A was associated with increasing the liver cirrhosis risk. Mol. Genet. Genomic Med. *7*, e543.

iScience, Volume *23*

Supplemental Information

FAM13A Represses AMPK Activity and Regulates Hepatic Glucose and Lipid Metabolism

Xin Lin, Yae-Huei Liou, Yujun Li, Lu Gong, Yan Li, Yuan Hao, Betty Pham, Shuang Xu, Zhiqiang Jiang, Lijia Li, Yifan Peng, Dandi Qiao, Honghuang Lin, Pengda Liu, Wenyi Wei, Guo Zhang, Chih-Hao Lee, and Xiaobo Zhou

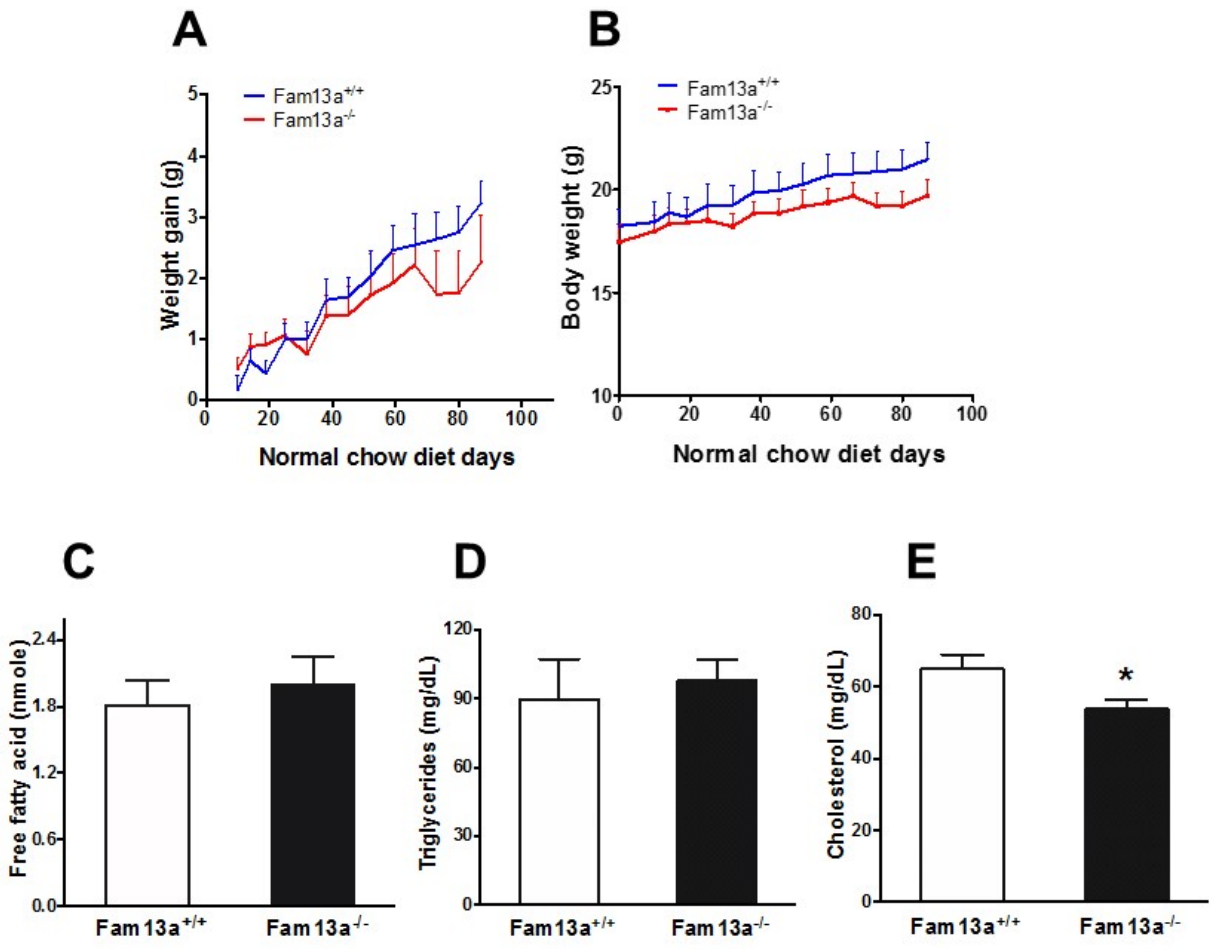

Figure S1. *Fam13a*$^{-/-}$ mice showed similar metabolic homeostasis in normal chow-fed female mice. Related to Figure 2.

Body weight gain of mice (**A**) and actual body weight (**B**) in normal chow-fed *Fam13a*$^{+/+}$ and Fam13a$^{-/-}$ mice for 3 months. Body weight was monitored every week from 8 weeks of age (n = 5-7 mice per group). Free fatty acid (**C**), triglycerides (**D**) and cholesterol (**E**) levels in *Fam13a*$^{+/+}$ and *Fam13a*$^{-/-}$ mice were assessed in serum from mice fasted overnight. Data are presented as mean ± SEM from 5-7 mice per genotype. *$p < 0.05$ by unpaired Student's *t*-test.

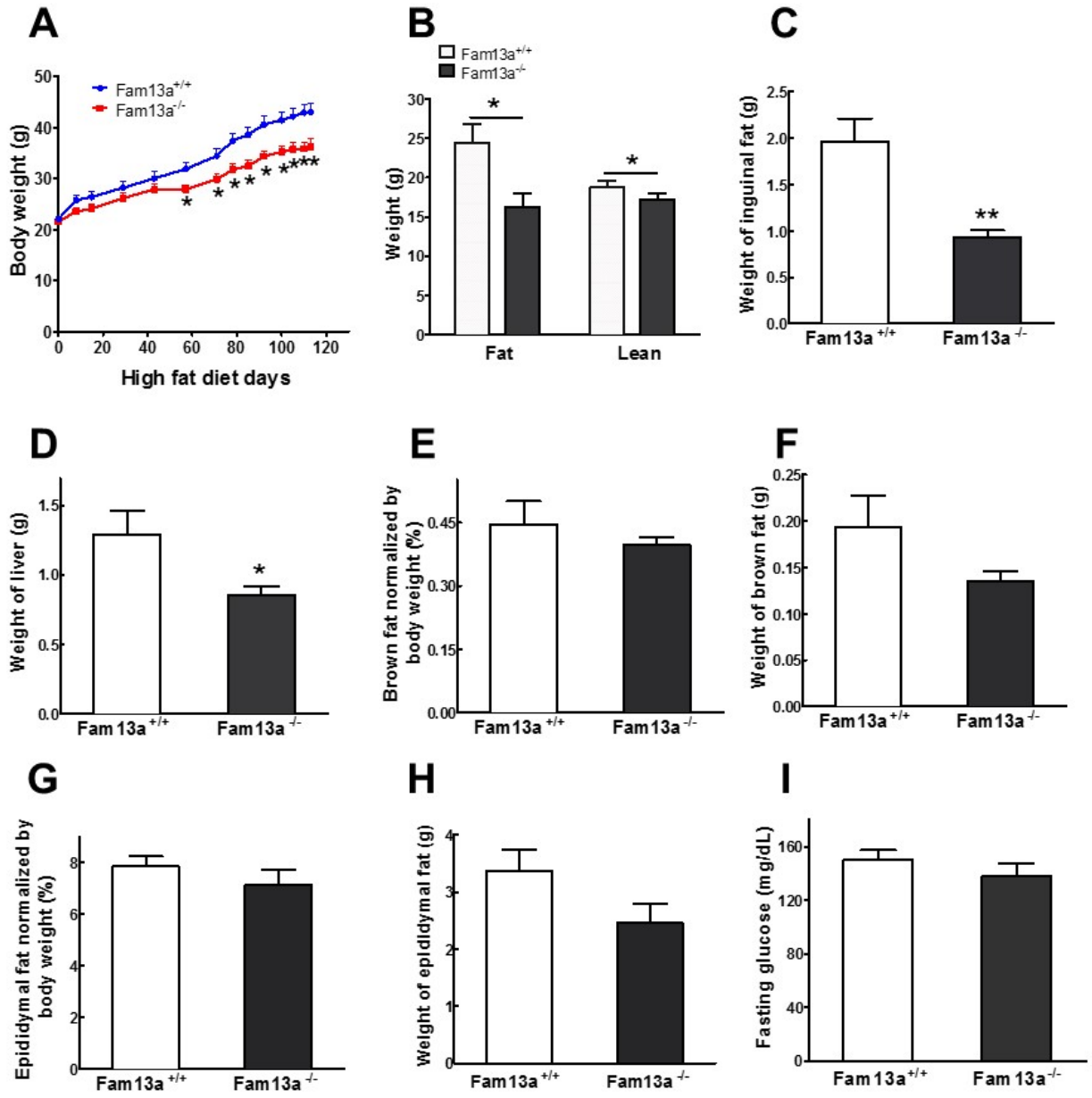

Figure S2. *Fam13a*$^{-/-}$ mice showed reduced body weight after high fat diet (HFD) treatment for 4 months. Related to Figure 2 and 3.

(**A**) Body weight was measured during HFD treatment for 4 months in *Fam13a*$^{+/+}$ (n = 13) and *Fam13a*$^{-/-}$ mice (n = 11). (**B**) Fat and lean mass of mice (**A**) measured by MRI after 4 months of HFD treatment. Weight of inguinal fat (**C**) and liver (**D**) in mice treated with HFD (n = 6 for *Fam13a*$^{+/+}$; n = 5 for *Fam13a*$^{-/-}$). Brown fat (**E**) and epididymal fat (**G**) mass normalized to body weight in mice treated with HFD. Weight of brown fat (**F**) and epididymal fat (**H**) were assessed with HFD-fed mice for 4 months (n = 6 for *Fam13a*$^{+/+}$; n = 5 for *Fam13a*$^{-/-}$). (**I**) Blood glucose was measured after fasting overnight in mice treated with HFD for 14 weeks (n = 6 for *Fam13a*$^{+/+}$; n = 5 for *Fam13a*$^{-/-}$). Data are presented as mean ± SEM. *p < 0.05 by unpaired Student's *t*-test. HFD: high fat diet.

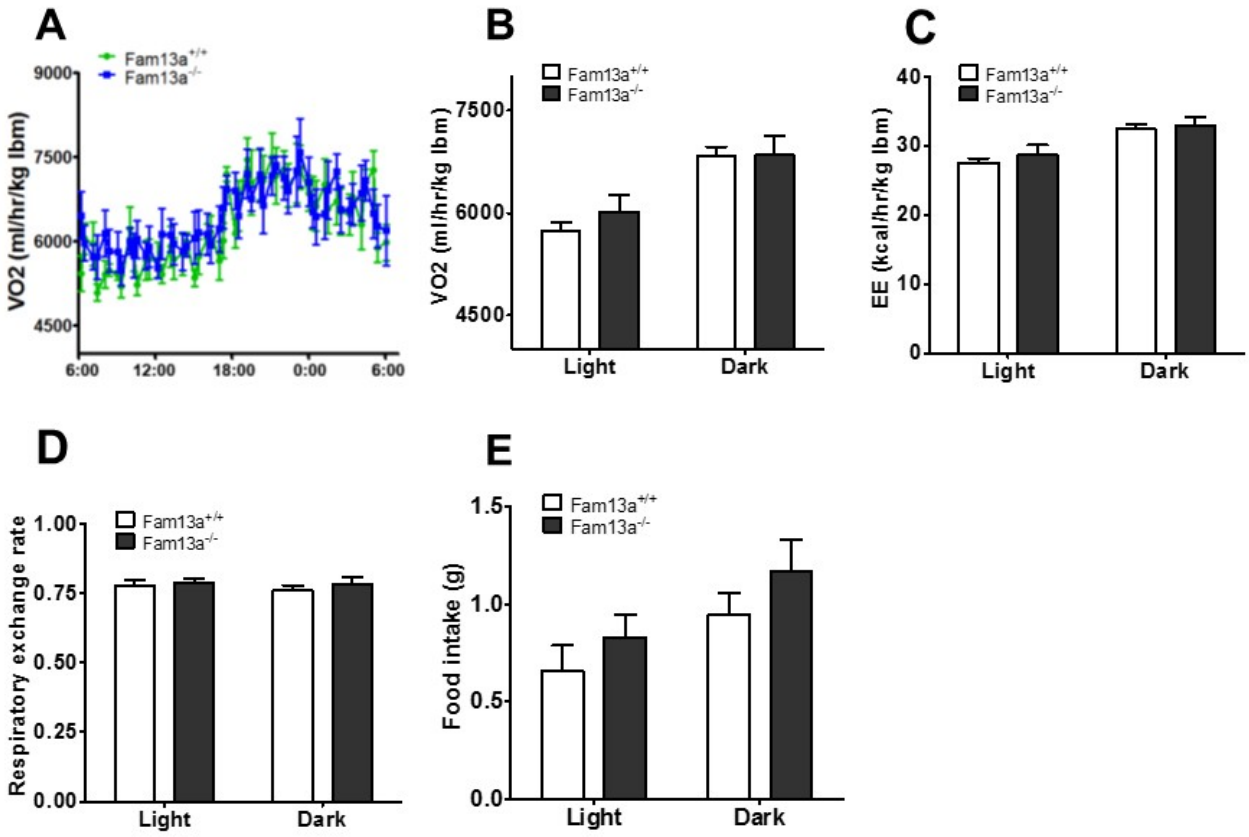

Figure S3. **Metabolic cage measurements in *Fam13a*$^{-/-}$ mice after HFD treatment for 7 weeks. Related to Figure 2.**

Oxygen consumption (**A and B**), energy expenditure (**C**), respiratory exchange rate (**D**) and food intake (**E**) were analyzed in *Fam13a*$^{+/+}$ and *Fam13a*$^{-/-}$ mice (n = 6 mice/genotype). Data are presented as mean ± SEM. HFD: high fat diet; VO2: oxygen consumption; EE: energy expenditure.

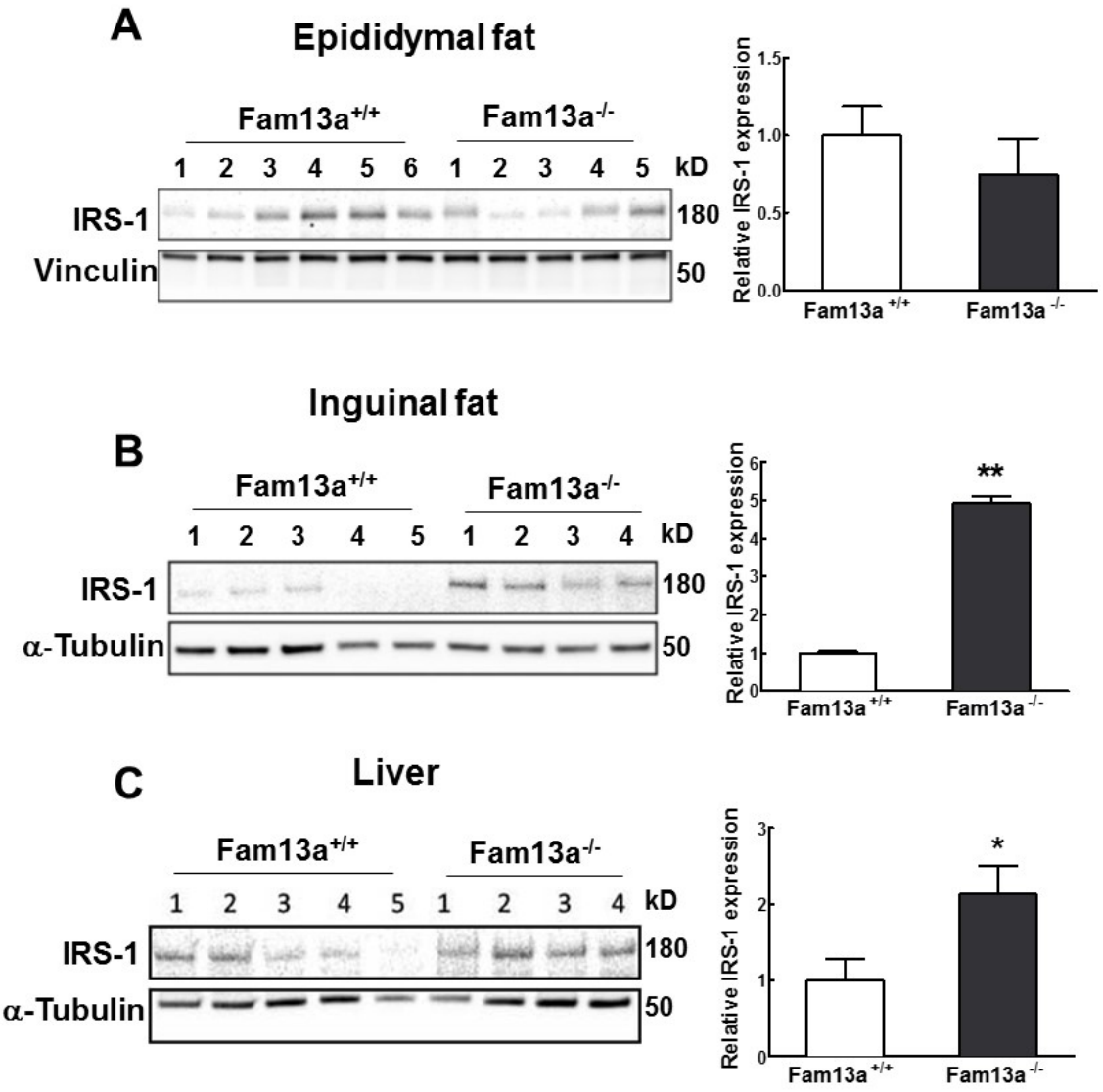

Figure S4. Protein levels of IRS-1 was determined by immunoblotting in epididymal fat (A), inguinal fat (B) and liver (C) from HFD-fed *Fam13a*$^{+/+}$ and *Fam13a*$^{-/-}$ mice for 4 months. Related to Figure 3. Quantifications were shown on the right with mean ± SEM from 4-6 mice per group. *p < 0.05 or **p < 0.01 by unpaired Student's *t*-test. HFD: high fat diet.

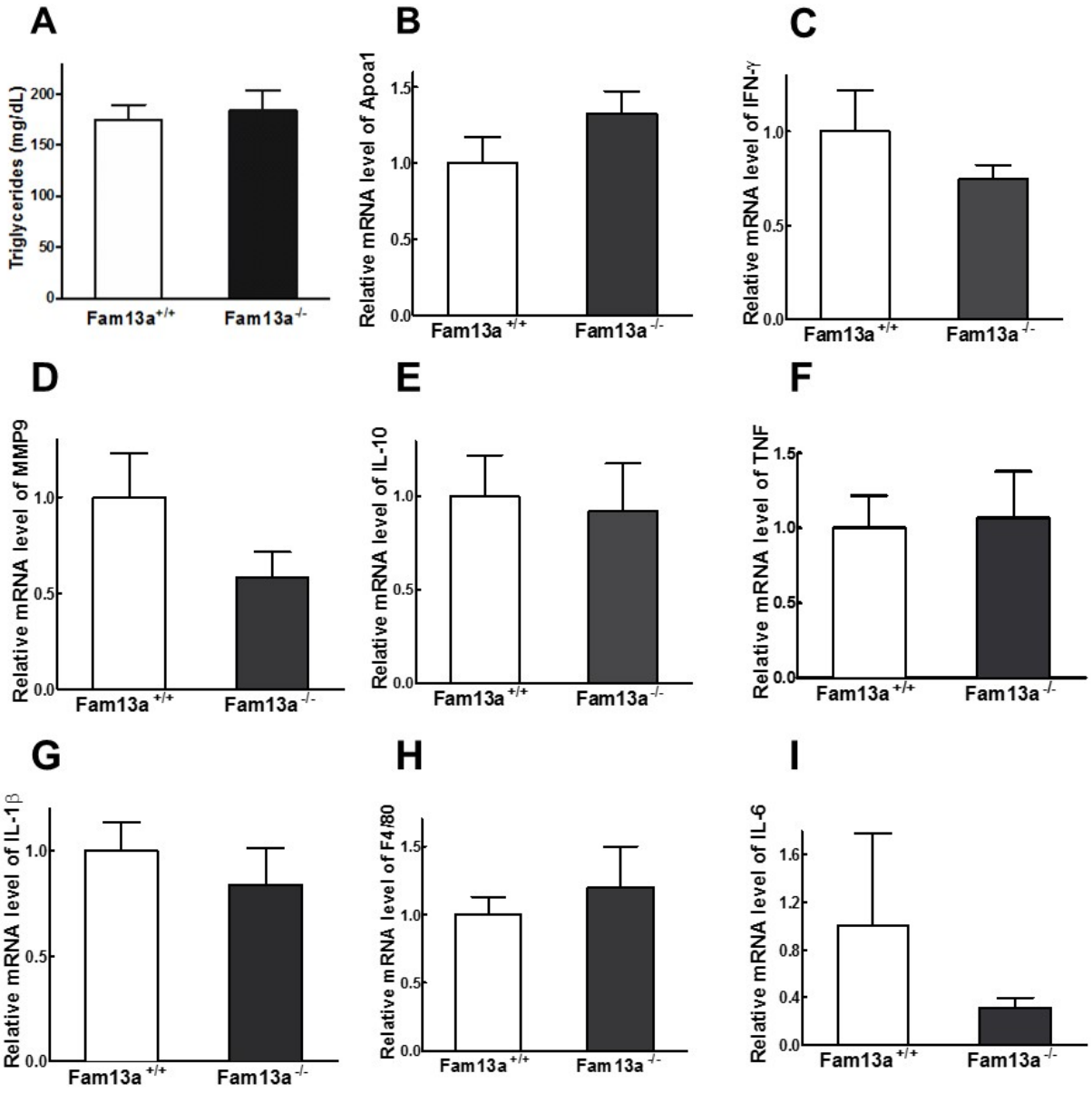

Figure S5. Triglycerides and gene expression measurements in the liver samples from HFD-fed *Fam13a*$^{+/+}$ and *Fam13a*$^{-/-}$ mice for 4 months. Related to Figure 4.

(**A**) Triglycerides levels were determined in serum from HFD-fed *Fam13a*$^{+/+}$ and *Fam13a*$^{-/-}$ mice. Expression of Apoa1 (**B**), IFN-γ (**C**), MMP9 (**D**), IL-10 (**E**), TNF (**F**), IL-1β (**G**), F4/80 (**H**) and IL-6 (**I**) were assessed by real-time PCR. Data are presented as mean ± SEM from 5-6 mice per group. HFD: high fat diet.

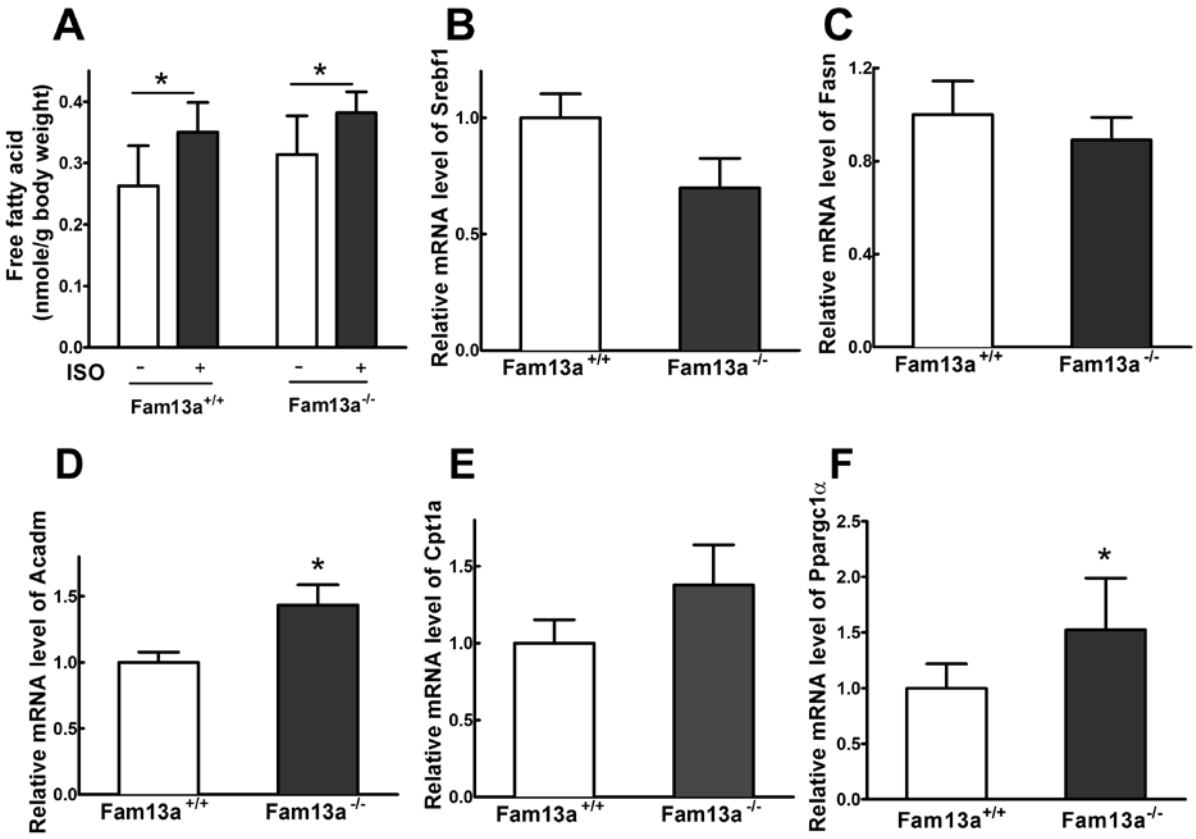

Figure S6. Regulation of lipolysis and oxidative metabolism in *Fam13a*$^{+/+}$ and *Fam13a*$^{-/-}$ mice. Related to Figure 5.

(**A**) Free fatty acid was measured in serum from normal chow-fed *Fam13a*$^{+/+}$ and *Fam13a*$^{-/-}$ female mice with or without isoproterenol-, a β3-adrenergic receptor agonist. Data are presented as mean ± SEM from 6 mice per group. *$p < 0.05$ vs. no ISO by two-way ANOVA. **ISO**: isoproterenol. mRNA levels of Srebf1 (**B**), Fasn (**C**), Acadm (**D**) and Cpt1a (**E**) were determined in the liver tissues from HFD-fed *Fam13a*$^{+/+}$ and *Fam13a*$^{-/-}$ mice for 4 months. (n = 6 for *Fam13a*$^{+/+}$; n = 5 for *Fam13a*$^{-/-}$). (**F**) Expression of Ppargc1α from primary hepatocytes was shown. Data are presented as mean ± SEM. *$p < 0.05$ by unpaired Student's *t*-test. HFD: high fat diet.

Table S1. **Association of MPRA SNPs in the FAM13A GWAS locus with HDL level. Related to Figure 1.** Three SNPs shown significant association at genome-wide levels were indicated by bold.

Chr Pos	SNP	A1	A2	beta	N	HDL P-value	Freq.A1.1000G.EUR
chr4:89726283	**rs2276936**	a	c	0.022	181105	**9.6E-10**	0.5
chr4:89726283	**rs2276936**	a	c	0.022	181105	**9.6E-10**	0.5
chr4:89737558	**rs7695177**	c	g	0.023	94311	**3.04E-06**	NA
chr4:89737558	**rs7695177**	c	g	0.023	94311	**3.04E-06**	NA
chr4:89730074	**rs2167750**	c	t	0.022	94311	**5.19E-06**	0.504
chr4:89730074	**rs2167750**	c	t	0.022	94311	**5.19E-06**	0.504
chr4:89730074	**rs2167750**	c	t	0.022	94311	**5.19E-06**	0.504
chr4:89730074	**rs2167750**	c	t	0.022	94311	**5.19E-06**	0.504
chr4:89734587	rs1350506	t	c	0.022	94311	0.000103	0.5013
chr4:89885086	rs2013701	g	t	0.009	91319	0.08229	0.5
chr4:89885086	rs2013701	g	t	0.009	91319	0.08229	0.5
chr4:89885086	rs2013701	g	t	0.009	91319	0.08229	0.5
chr4:89885086	rs2013701	g	t	0.009	91319	0.08229	0.5
chr4:89883979	rs7671167	c	t	0.009	91319	0.08721	0.4987
chr4:89883979	rs7671167	c	t	0.009	91319	0.08721	0.4987
chr4:89883979	rs7671167	c	t	0.009	91319	0.08721	0.4987
chr4:89986326	rs6857969	a	g	0.006	94311	0.2168	0.3404
chr4:89986326	rs6857969	a	g	0.006	94311	0.2168	0.3404
chr4:89986326	rs6857969	a	g	0.006	94311	0.2168	0.3404
chr4:89998258	rs874147	a	c	0.006	91202	0.229	0.3443
chr4:89930313	rs1795739	g	a	0.004	91319	0.3556	0.6161
chr4:89930313	rs1795739	g	a	0.004	91319	0.3556	0.6161
chr4:90036099	rs12645173	g	a	0.006	94311	0.4808	0.3575
chr4:89921981	rs7656238	t	c	0.004	94311	0.4848	0.7863
chr4:89918968	rs10516826	c	t	0.005	94311	0.5262	0.8285
chr4:90077431	rs7672894	t	a	0.002	94311	0.604	1
chr4:90077431	rs7672894	t	a	0.002	94311	0.604	1
chr4:90077431	rs7672894	t	a	0.002	94311	0.604	1
chr4:90077431	rs7672894	t	a	0.002	94311	0.604	1
chr4:90077431	rs7672894	t	a	0.002	94311	0.604	1

chr4:89919413	rs2869972	a	g	0.003	94311	0.6438	0.7863
chr4:89919413	rs2869972	a	g	0.003	94311	0.6438	0.7863
chr4:90059434	rs6828137	g	t	0.003	94291	0.7704	0.5435
chr4:90059434	rs6828137	g	t	0.003	94291	0.7704	0.5435
chr4:89930434	rs1795738	t	c	0.002	94288	0.7948	0.7916
chr4:89930434	rs1795738	t	c	0.002	94288	0.7948	0.7916
chr4:89727979	rs10516821	c	t	8E-04	71228	0.8077	0.05937
chr4:89727979	rs10516821	c	t	8E-04	71228	0.8077	0.05937
chr4:89854079	rs4693977	t	a	9E-04	94311	0.8814	1
chr4:89973910	rs2670623	a	g	9E-04	94311	0.8974	0.8021
chr4:89938362	rs12508524	a	g	3E-04	94283	0.9125	0.2876

Chr Pos: Chromsome position of a given variant.
SNP: Single nucleotide polymorphism.
A1 and A2: two opposing alleles for each given variant.
Freq.A1.1000G.EUR: Allele frequlnecy of the major allele for each variant
N: Subject number for each genotype of a given variant.

Table S2. **Association of three significant HDL and MPRA SNPs near FAM13A gene with body fat distribution and whole-body fat mass in subjects from UK Biobank. Related to Figure 1.**

SNP	Trait	P-value	Beta	N Overall	Variant	Effect allele
rs2167750	Body fat percentage	1.32E-12	-0.0132542	331117	4_89730074_C_T	T
rs2167750	Impedance of arm (right)	1.58E-12	-0.012114	331279	4_89730074_C_T	T
rs2167750	Hip circumference	1.90E-12	-0.0169994	336601	4_89730074_C_T	T
rs2167750	Arm fat percentage (left)	5.82E-11	-0.0120825	331198	4_89730074_C_T	T
rs2167750	Trunk fat mass	6.32E-10	-0.0151724	331093	4_89730074_C_T	T
rs2167750	Arm fat percentage (right)	1.02E-09	-0.0113193	331249	4_89730074_C_T	T
rs2167750	Whole body fat mass	1.49E-08	-0.0134662	330762	4_89730074_C_T	T
rs2276936	Trunk fat percentage	1.43E-13	-0.0165482	331113	4_89726283_A_C	C
rs2276936	Impedance of arm (left)	5.22E-13	-0.0124158	331292	4_89726283_A_C	C
rs2276936	Hip circumference	2.44E-12	-0.0168992	336601	4_89726283_A_C	C
rs2276936	Body fat percentage	2.53E-12	-0.013072	331117	4_89726283_A_C	C
rs2276936	Impedance of arm (right)	7.39E-12	-0.0117307	331279	4_89726283_A_C	C
rs2276936	Arm fat percentage (left)	7.33E-11	-0.0120074	331198	4_89726283_A_C	C
rs2276936	Arm fat percentage (right)	8.99E-10	-0.0113457	331249	4_89726283_A_C	C
rs2276936	Trunk fat mass	9.69E-10	-0.0149921	331093	4_89726283_A_C	C
rs2276936	Whole body fat mass	1.77E-08	-0.0133836	330762	4_89726283_A_C	C
rs7695177	Trunk fat percentage	2.04E-13	-0.0164525	331113	4_89737558_C_G	G
rs7695177	Hip circumference	1.82E-12	-0.017008	336601	4_89737558_C_G	G
rs7695177	Impedance of arm (left)	2.66E-12	-0.0120368	331292	4_89737558_C_G	G
rs7695177	Body fat percentage	3.98E-12	-0.0129615	331117	4_89737558_C_G	G
rs7695177	Impedance of arm (right)	2.18E-11	-0.01147	331279	4_89737558_C_G	G
rs7695177	Arm fat percentage (left)	9.11E-11	-0.0119544	331198	4_89737558_C_G	G
rs7695177	Arm fat percentage (right)	9.45E-10	-0.0113377	331249	4_89737558_C_G	G
rs7695177	Trunk fat mass	1.36E-09	-0.0148679	331093	4_89737558_C_G	G

Table S3. The primers used for molecular cloning of reporter constructs. Related to Figure 1.
FWD: forward orientation; REV: reverse orientation

Primers	Sequence	Product (bp)
FAM13A Promoter-FWD	GAAGTGATGGTCTGGACTATGTT	920
FAM13A Promoter-REV	CTACTCCTTCTGCTCCTCAATG	920
rs2167750-WT-FWD-C	TGAAACAACTTAGAATTCATTCGATTTCC	538
rs2167750-MUT-FWD-T	TGTAGCTTCTTAGATTTAGACTATTATTTAGGTCTATATGATAAATGTTCTTCC	538
rs2167750-WT-REV-G	TTCTTAGACATATACAACACTATGCCTTTC	538
rs2167750-MUT-REV-A	GGAAGAACATTTATCATATAGACCTAAATAATAGTCTAAATCTAAGAAGCTACA	538
rs2276936-WT-FWD-A	CTCCAGCAAGTTAGTCTGGC	503
rs2276936-MUT-FWD-C	GGCTTTAATGTGCTAAATCAACATTTTTGACAGGTAGAACATTTTTAGTAAAATTGA	503
rs2276936-WT-REV-T	AGTATGTAATCATTTTAAGGGTTTATGTGT	503
rs2276936-MUT-REV-G	TCAATTTTACTAAAAATGTTCTACCTGTCAAAAATGTTGATTTAGCACATTAAAGCC	503
rs7695177-WT-FWD-C	ATAGGAACTTCATTTTCCTTAAACTGC	501
rs7695177-MUT-FWD-G	AAGCATATCAGAACACTATTGTCCACATAATTTCTAAAGCTTTCCAT	501
rs7695177-WT-REV-G	AGGGAAGAGTCTATTGTCATTCAAAA	501
rs7695177-MUT-REV-C	ATGGAAAGCTTTAGAAATTATGTGGACAATAGTGTTCTGATATGCTT	501

Table S4. Sequence of gRNAs used for deletion generation nearby the rs2276936. Related to Figure 1.

Primers	Sequence	Deletion size (~bp)
Rs227-1 upper	5’-CACCGTTATTTTCCTTTTAGTTCAC-3’	148
Rs227-1 lower	5’-CACCGTAGTAAAACATGATCCACCT-3’	148
Rs227-2 upper	5’-CACCGTTATTTTCCTTTTAGTTCAC-3’	117
Rs227-2 lower	5’-CACCGCATTAAAGCCAATCACATGA-3’	117

TRANSPERENT METHODS

Open Chromatin Region Analysis

All liver-related and publicly available datasets of ATAC-Seq and DNase-Seq (bigwig files) were generated from Roadmap Epigenomics Project (Ernst and Kellis, 2015; Kundaje et al., 2015) and The Encyclopedia of DNA Elements (ENCODE) project (Inoue et al., 2017; Kazachenka et al., 2018). The genomic region of 89,706,500 - 89,752,000 on Chromatin 4 (GRCh37/hg19 as the reference genome) was shown with signal intensities across selected epigemonic datasets with IGV at version 2.5.3 (Broad Institute). Total open chromatin score was calculated as the mean value of all corresponding used datasets.

Animals

All animal studies were performed under the guidelines for the treatment of laboratory animals and approved by the Institutional Animal Care and Use Committee, Brigham and Women's Hospital. *Fam13a*$^{-/-}$ mice in the C57BL/6 background were generated as previously described (Jiang et al., 2016). Briefly, Fam13a knockout embryonic stem cells in C57Bl/6 N background were injected to C57BL/6 J mice for germline transmission followed by ~3 generation of crossing into C57BL/6 J background. Background- and age-matched littermates were used as *Fam13a*$^{+/+}$ controls. Normal chow- (containing 5.6% fat and 20% protein) fed *Fam13a*$^{-/-}$ and *Fam13a*$^{+/+}$ mice were performed in 2 groups (n = 5-7 per genotype, 2-5 months old). Four-to five-months-old female mice were fed with HFD containing 36% fat, 35.7% carbohydrates, and 20.5% protein (F3282, Bio-Serv, Flemington, NJ) for 4 months. Two batches of experimental repeats were performed with 5-6 mice/group in each repeat. These mice were fed ad libitum and housed in a quiet room without disturbance of their sleep/wake behavior to reduce environmental stress in the animal facility of Brigham and Women's Hospital.

Metabolic Studies

To determine roles of FAM13A in hepatic insulin signaling, insulin (5 U/kg, R-100, Eli Lilly and Company, Indianapolis, IN) was injected through the portal vein in mice after overnight fasting and tissue samples were collected before and 5 minutes after insulin injection as described previously (Jacobi et al., 2015). Briefly, a piece of liver was tied tightly by suture and then removed before insulin injection with no bleeding. Five minutes later after injection, another piece of liver sample was also collected in the same animal. Body compositions of mice including lean mass and fat mass were measured in mice using magnetic resonance imaging (MRI) by Brigham and Women's Metabolic Core. Oxygen consumption (VO2), energy expenditure (EE), respiratory exchange rate and food intake were measured in mice fed with HFD for 7 weeks by Brigham and Women's Metabolic Core. Lipolysis assay was performed as previously described (Rohm et al., 2013). Briefly, mice were fasted overnight with free access to water. Isoproterenol (I6504, Millipore Sigma, St. Louis, MO) dissolved freshly in PBS was injected by i.p. at 10 mg/kg body weight. Thirty minutes later, plasma samples were collected and free fatty acid was measured with free fatty acid quantification kit (MAK044, Millipore Sigma, St. Louis, MO). Fasting glucose was determined after overnight fasting. ITT (Insulin tolerance test) and GTT (Glucose tolerance test) were performed as described previously (Stanya et al., 2013) with human insulin (1 U/kg) (R-100, Eli Lilly and Company, Indianapolis, IN) after a 6-hour fasting or glucose (1.5 g/kg) after overnight fasting by i.p. injection, respectively. Blood glucose was measured before and after injection at the indicated time points using a glucometer (FreeStyle Precision Neo). Insulin concentrations in serum was measured using a commercial kit (EZRMI-13K, Millipore Sigma, St. Louis, MO). Blood and hepatic free fatty acid (MAK044, Millipore Sigma, St. Louis, MO), triglycerides (TR22421, Thermo Scientific, Waltham, MA) and cholesterol (ab65390, Abcam, Cambridge, MA) levels were measured using commercial kits based on manufacturer's instruction. Hepatic lipids were extracted as described previously (Akiyama et al., 2004; Liu et al., 2011). Frozen liver samples (10-20 mg) were

homogenized in 500 μl lysis buffer (50 mM Tris (pH 8.0), 100 mM NaCl and 0.1% NP40) and then dried using Speed Vacuum. Lipids were thus extracted from dried tissues by chloroform: methanol (2:1 V/V) followed by measurements on free fatty acid, triglycerides and cholesterol assays using kits as described above.

Primary hepatocytes isolation and glucose production assays

Primary hepatocytes were isolated from anesthetized animals perfused with a collagenase solution (Liberase TM, Roche, Basel, Switzerland) in situ through the portal vein (Liu et al., 2013). Cells were liberated into DMEM after perfusion. A 45% Percoll (GE Lifescience, Marlborough, MA) gradient was used to separate live and dead hepatocytes. For glucose production measurements ex vivo, murine hepatocytes were cultured in DMEM with glucose (1.5 g/L) for 2 hours after serum withdrawal. Cells were then incubated in glucose production media (DMEM without glucose or phenol red, supplemented with 4 mM L-glutamine, 1 mM pyruvate and 10 mM sodium lactate) for 4 hours. Glucose concentrations in the media were measured by glucose assay kit (GAGO-20, Millipore Sigma, St. Louis, MO). Total protein amount of hepatocyte was measured by BCA protein assays (Thermo Scientific, Waltham, MA) for normalization.

Measurements of Mitochondrial Respiration

Extracellular Flux Analyzer (Seahorse Bioscience) was used to measure oxygen consumption rate (OCR), an indicator of mitochondrial respiration, in primary murine hepatocytes and HepG2 cells. Briefly, isolated hepatocytes or HepG2 cells were seeded directly into XF24 plates at a density of 2.5 x 10^4 or 4 x 10^4 cells/well, respectively. Mitochondrial respiration was measured on the next day in Agilent Seahorse XF Base Medium (Agilent Technologies) supplemented with pyruvate (10 mM) using the Seahorse XF Cell Mito Stress Test program. During the assay, oligomycin (2 mM), carbonyl cyanide-4-(trifluoromethoxy) phenylhydrazone (FCCP, 1 mM) and actinomycin/rotenone (1 mM of

each) were sequentially added into each well for measurements on basal respiration, ATP production, maximum respiration, and proton leak (complex I driven), respectively.

Histology

Liver samples were fixed with 10% buffered formalin and embedded in paraffin. Hematoxylin and eosin staining was performed by InvivoEx LLC (InvivoEx LLC, Waltham, MA).

Cell culture and transfection

Embryonic kidney epithelial cells (HEK 293) and human hepatoma HepG2 cells were obtained from ATCC (American Type Culture Collection) and cultured in Dulbecco's modified Eagle medium or Eagle's Minimal Essential Medium (EMEM), respectively, supplemented with 10% fetal bovine serum, penicillin (50 units/ml), and streptomycin (50 μg/ml). Expression constructs of Flag/Myc-tagged FAM13A (NP_001252507.1) (Jiang et al., 2016) and HA-tagged AMPKα1 or AMPKα2 (Wan et al., 2018) were transfected into cells using lipofectamine 3000 (Invitrogen, Carlsbad, CA) as the manufacturer recommended. Cells were used for various experiments 48 hours after transfection.

RNA interference

HepG2 cells were transfected with 50 nM FAM13A siRNA (L-020516-00-0020, Lafayette, CO) or non-target control siRNA (D-001810-10-20, Lafayette, CO) using Lipofectamine RNAiMAX transfection reagent (13778150, Thermo Scientific, Waltham, MA) according to the manufacturer's instruction. Samples were harvested 48 hours after transfection. To produce FAM13A and AMPK shRNA containing lentivirus, HEK293T cells were co-transfected lentiFAM13A shRNA (1007266a, abmgood, Richmond, BC, Canada) and/or lentiAMPK shRNA (1000086a, abmgood, Richmond, BC, Canada) with psPAX2 and pMD2.G using lipofectamine 3000. Lentiviruses were collected after 48

h and then infected HepG2 cells for 24 h in the presence of 8 μg/ml polybrene (TR-1003-G, Millipore Sigma, Burlington, MA) and selected with 2 μg/ml of puromycin (P8833, Millipore Sigma, Burlington, MA).

RNA Extraction and Quantitative Real-time PCR

Total RNA was extracted from cells or frozen tissues using QIAzol lysis reagent (79306, Qiagen, Venlo, Netherlands) and the RNeasy mini kit (74106, Qiagen, Venlo, Netherlands). cDNA was obtained using high-capacity cDNA reverse transcription kit (4374966, Thermo Scientific, Waltham, MA). Relative gene expression was conducted by real-time PCR using TaqMan assays (4444964, Thermo Scientific, Waltham, MA) in a QuantStudio 12K machine (Life Technologies, Carlsbad, CA) and normalized to Rplp0 expression. TaqMan probes purchased from Integrated DNA Technologies (IDT, Skokie, IL) including human FAM13A (Hs.PT.58.1607079), human GAPDH (Hs.PT.39a.22214836), mouse FAM13A (Mm.PT.56a.42496772), mouse Fasn (Mm.PT.58.41299055), mouse Apoa1 (Mm.PT.58.11772461), mouse Srebf1 (Mm.PT.58.8508227), mouse IL-6 (Mm.PT.58.10005566), mouse IFN-γ (Mm.PT.58.41769240), mouse MMP-9 (Mm.PT.58.10100097), mouse IL-10 (Mm.PT.58.13531087), mouse TNF (Mm.PT.58.12575861), mouse IL-1β (Mm.PT.58.41616450), mouse F4/80 (Mm.PT.58.11087779), mouse Acadm (Mm.PT.58.9316361), mouse Ppargc1α (Mm.PT.58.16192665), mouse Cpt1a (Mm.PT.58.10147164) and mouse Rplp0 (Mm.PT.58.43894205). All samples were assayed in duplicate in quantitative real-time PCR. Expression levels of target genes were calculated based on the $2^{-\Delta\Delta Ct}$ method.

Molecular Cloning and Reporter Assays

We engineered reporter constructs for each of the three SNPs (rs2167750, rs2276936, and rs7695177) into pGL4.32 luciferase construct. SNP-containing oligonucleotides were cloned into the pGL3-Basic

vector (Promega, Madison, WI) and the FAM13A promoter was inserted to the upstream of the luciferase gene. The primer sequences are shown in Supplementary Table 3. For each SNP, we tested both forward and reverse orientations, resulting in 4 unique oligonucleotide contexts. All plasmids used for reporter assays were confirmed by sequencing. We performed reporter assays in HepG2 cells as previously described (Castaldi et al., 2019). Briefly, 70% confluent HepG2 cells were plated into a 24-well plate. Eighteen hours later, cells were collected to measure enhancer activity using the Dual-Luciferase Reporter Assay System (E1960, Promega, Madison, WI) according to the manufacturer's protocol. Luminescence signals were captured in GloMax GM2010 plate reader (Promega, Madison, WI). Independent transfection and reporter assays (triplicates) were performed four times.

CRISPR/CAS9 FAM13A Gene Knockout

To generate the DNA regional deletion spanning rs2276936, we designed 2 pairs of gRNA (rs227-1 and rs227-2) encompassing this SNP. The sequences of gRNAs are shown in Supplementary Table 4. gRNA pairs were cloned into pSpCas9 (BB)-2A-Puro (PX459) V2.0 vectors (Addgene #62988). To generate the small indel deletion nearby rs2276936, single guide RNA (5'-GCTAAATCAACATTTTTTAC-3') spanning this SNP was cloned into PX459 and confirmed by sequencing. PX459 constructs with or without gRNA were transfected into HepG2 cells with Lipofectamine 3000 (L3000015, Fisher Scientific, Hampton, NH). After puromycin (ant-pr-1, InvivoGen, San Diego, CA) selection at 1.5 µg/mL, cells were recovered for 3-5 days and expanded for RNA extraction and quantitative real-time PCR.

Immunoblotting

Cells and tissues were lysed in lysis buffer with protease inhibitor cocktail (11697498001, Millipore Sigma, St. Louis, MO) and phosphatase inhibitor (NC0831193, Fisher Scientific, Hampton, NH). Lysates were cleared by centrifugation at 4°C at 14,000 rpm for 10 mins and protein concentrations

were determined by the Bradford method. Antibodies against the following proteins were used for western blotting: p-Akt (Thr308, #2965), Akt (#4691), p-AMPK (Thr172, #2535), AMPK (#2532), IRS-1 (#2382) from Cell Signaling (Danvers, MA). Anti-flag (#F1804) and anti-vinculin (#V-4505) antibodies were from Millipore Sigma (St. Louis, MO). Anti-FAM13A (#ab122440), anti-β-Actin (#ab20272) and anti-α-Tubulin (#ab185067) were obtained from Abcam (Cambridge, MA). Anti-Myc (#05-419) was purchased from Millipore (Burlington, MA). Densitometry of immunoblotting was analyzed using NIH Image J software.

Statistical Analyses

Statistics analyses were performed using unpaired Student's *t* test. Data are presented as means ± SEM for *in vivo* studies. For *in vitro* assays, means ± SD were obtained from at least three biological replicates. Significance was claimed if established at $p < 0.05$.

Supplemental References

Akiyama, T.E., Lambert, G., Nicol, C.J., Matsusue, K., Peters, J.M., Brewer, H.B., Jr., and Gonzalez, F.J. (2004). Peroxisome proliferator-activated receptor beta/delta regulates very low density lipoprotein production and catabolism in mice on a Western diet. J Biol Chem *279*, 20874-20881.

Castaldi, P.J., Guo, F., Qiao, D., Du, F., Naing, Z.Z.C., Li, Y., Pham, B., Mikkelsen, T.S., Cho, M.H., Silverman, E.K., *et al.* (2019). Identification of Functional Variants in the FAM13A Chronic Obstructive Pulmonary Disease Genome-Wide Association Study Locus by Massively Parallel Reporter Assays. Am J Respir Crit Care Med *199*, 52-61.

Ernst, J., and Kellis, M. (2015). Large-scale imputation of epigenomic datasets for systematic annotation of diverse human tissues. Nat Biotechnol *33*, 364-376.

Inoue, F., Kircher, M., Martin, B., Cooper, G.M., Witten, D.M., McManus, M.T., Ahituv, N., and Shendure, J. (2017). A systematic comparison reveals substantial differences in chromosomal versus episomal encoding of enhancer activity. Genome Res *27*, 38-52.

Jacobi, D., Liu, S., Burkewitz, K., Kory, N., Knudsen, N.H., Alexander, R.K., Unluturk, U., Li, X., Kong, X., Hyde, A.L., *et al.* (2015). Hepatic Bmal1 Regulates Rhythmic Mitochondrial Dynamics and Promotes Metabolic Fitness. Cell Metab *22*, 709-720.

Jiang, Z., Lao, T., Qiu, W., Polverino, F., Gupta, K., Guo, F., Mancini, J.D., Naing, Z.Z., Cho, M.H., Castaldi, P.J., *et al.* (2016). A Chronic Obstructive Pulmonary Disease Susceptibility Gene, FAM13A, Regulates Protein Stability of beta-Catenin. Am J Respir Crit Care Med *194*, 185-197.

Kazachenka, A., Bertozzi, T.M., Sjoberg-Herrera, M.K., Walker, N., Gardner, J., Gunning, R., Pahita, E., Adams, S., Adams, D., and Ferguson-Smith, A.C. (2018). Identification, Characterization, and Heritability of Murine Metastable Epialleles: Implications for Non-genetic Inheritance. Cell *175*, 1259-1271 e1213.

Kundaje, A., Meuleman, W., Ernst, J., Bilenky, M., Yen, A., Heravi-Moussavi, A., Kheradpour, P., Zhang, Z., Wang, J., Ziller, M.J., *et al.* (2015). Integrative analysis of 111 reference human epigenomes. Nature *518*, 317-330.

Liu, S., Brown, J.D., Stanya, K.J., Homan, E., Leidl, M., Inouye, K., Bhargava, P., Gangl, M.R., Dai, L., Hatano, B., *et al.* (2013). A diurnal serum lipid integrates hepatic lipogenesis and peripheral fatty acid use. Nature *502*, 550-554.

Liu, S., Hatano, B., Zhao, M., Yen, C.C., Kang, K., Reilly, S.M., Gangl, M.R., Gorgun, C., Balschi, J.A., Ntambi, J.M., *et al.* (2011). Role of peroxisome proliferator-activated receptor {delta}/{beta} in hepatic metabolic regulation. J Biol Chem *286*, 1237-1247.

Rohm, M., Sommerfeld, A., Strzoda, D., Jones, A., Sijmonsma, T.P., Rudofsky, G., Wolfrum, C., Sticht, C., Gretz, N., Zeyda, M., *et al.* (2013). Transcriptional cofactor TBLR1 controls lipid mobilization in white adipose tissue. Cell Metab *17*, 575-585.

Stanya, K.J., Jacobi, D., Liu, S., Bhargava, P., Dai, L., Gangl, M.R., Inouye, K., Barlow, J.L., Ji, Y., Mizgerd, J.P., *et al.* (2013). Direct control of hepatic glucose production by interleukin-13 in mice. J Clin Invest *123*, 261-271.

Wan, L., Xu, K., Wei, Y., Zhang, J., Han, T., Fry, C., Zhang, Z., Wang, Y.V., Huang, L., Yuan, M., *et al.* (2018). Phosphorylation of EZH2 by AMPK Suppresses PRC2 Methyltransferase Activity and Oncogenic Function. Mol Cell *69*, 279-291 e275.